# Selective Cytotoxicity of the NAMPT Inhibitor FK866 Toward Gastric Cancer Cells With Markers of the Epithelial-Mesenchymal Transition, Due to Loss of NAPRT

Jooyoung Lee,[1,*] **Hyosil Kim,**[1,*] **Jae Eun Lee,**[1,2,*] Su-Jin Shin,[3] Sejin Oh,[1,4] Gino Kwon,[5] Hakhyun Kim,[1,4] Yoon Young Choi,[1,2] Michael A. White,[6] Soonmyung Paik,[1] Jae-Ho Cheong,[1,2,4,§] and Hyun Seok Kim[1,4,§]

[1]Severance Biomedical Science Institute, Yonsei University College of Medicine, Seoul, Korea; [2]Department of Surgery, Yonsei University College of Medicine, Seoul, Korea; [3]Department of Pathology, Hanyang University College of Medicine, Seoul, Korea; [4]Brain Korea 21 Plus Project for Medical Science, Yonsei University College of Medicine, Seoul, Korea; [5]Graduate Program for Nanomedical Science, Yonsei University, Seoul, Korea; and [6]Department of Cell Biology, University of Texas Southwestern Medical Center, Dallas, Texas
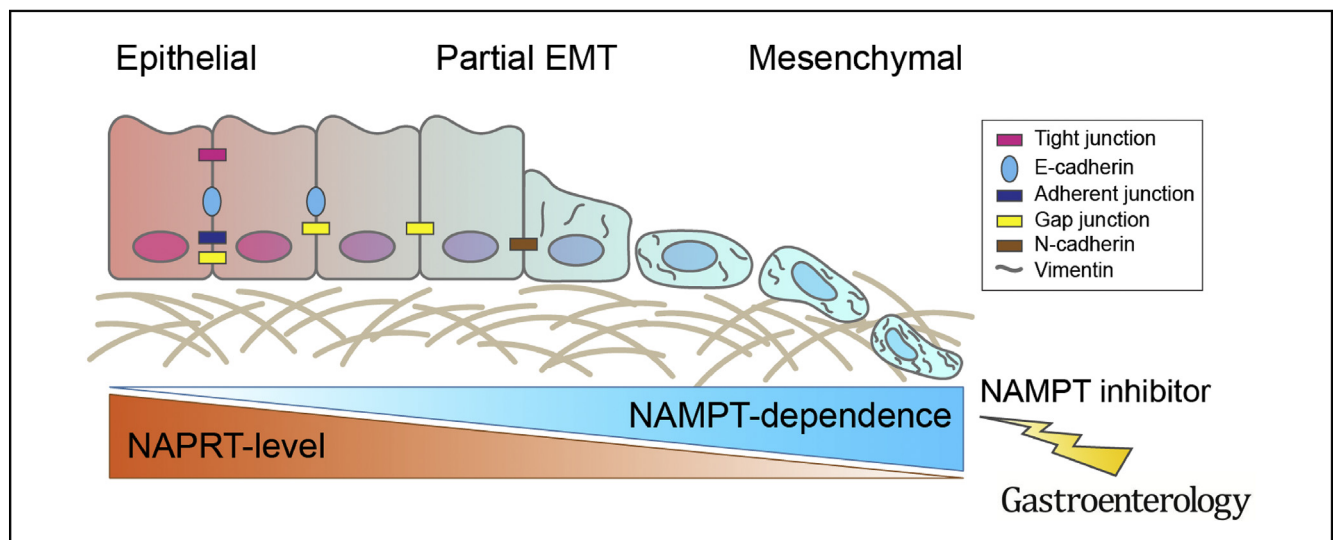
BACKGROUND & AIMS: Markers of the epithelial-to-mesenchymal transition (EMT) in gastric tumor tissues are associated with poor patient outcomes. We performed a screen to identify pharmacologic compounds that kill gastric cancer cells with EMT-associated gene expression patterns and investigate their mechanisms. **METHODS:** We identified 29 gastric cancer cell lines with a gene expression signature previously associated with an EMT subtype, based on data from RNA sequence analyses, and confirmed the mesenchymal phenotypes of 7 lines (Hs746T, SNU1750, MKN1, SK4, SNU484, SNU668, and YCC11), based on invasive activity and protein markers. We screened 1,345 compounds for their ability to kill cells with the EMT signature compared with cell lines without this pattern. We tested the effects of identified compounds in BALB/c nude mice bearing GA077 tumors; mice were given intraperitoneal injections of the compound or vehicle (control) twice daily for 24 days and tumor growth was monitored. Proteins associated with the toxicity of the compounds were overexpressed in MKN1 and SNU484 cells or knocked down in MKN45 and SNU719 using small interfering RNAs. We performed immunohistochemical analyses of 942 gastric cancer tissues and investigated associations between EMT markers and protein expression patterns. **RESULTS:** The nicotinamide phosphoribosyltransferase inhibitor FK866 killed 6 of 7 gastric cancer cell lines with EMT-associated gene expression signatures but not gastric cancer cells without this signature. The 6 EMT-subtype gastric cell lines expressed significantly low levels of nicotinic acid phosphoribosyltransferase (NAPRT), which makes the cells hypersensitive to nicotinamide phosphoribosyltransferase inhibition. Gastric cell lines that expressed higher levels of NAPRT, regardless of EMT markers, were sensitized to FK866 after knockdown of NAPRT, whereas overexpression of NAPRT in deficient EMT cell lines protected them from FK866-mediated toxicity. Administration of FK866 to nude mice with tumors grown from GA077 cells (human gastric cancer tumors of the EMT subtype) led to tumor regression in 2 weeks; FK866 did not affect tumors grown from MKN45 cells without the EMT expression signature. Loss of NAPRT might promote the EMT, because it stabilizes β-catenin. We correlated the EMT gene expression signature with lower levels of NAPRT in 942 gastric tumors from patients; we also found lower levels of *NAPRT* mRNA in colorectal, pancreatic, and lung adenocarcinoma tissues with the EMT gene expression signature. **CONCLUSIONS:** FK866 selectively kills gastric

cancer cells with an EMT gene expression signature by inhibiting nicotinamide phosphoribosyltransferase in cells with NAPRT deficiency. Loss of NAPRT expression, frequently through promoter hypermethylation, is observed in many gastric tumors of the EMT subtype. FK866 might be used to treat patients with tumors of this subtype.

Keywords: Stomach Cancer; Drug Screen; Partial Epithelial-to-Mesenchymal Transition; Synthetic Lethal.

G astric cancer is a leading cause of cancer-related death worldwide. Few targeted therapies for gastric cancer are available because pharmacologically tractable, recurrent mutations are rare in gastric cancer. In gastric cancer, molecular heterogeneity affects prognosis and treatment outcomes. Multiple classification methods have been developed to define gastric cancer molecular subtypes based on a set of heterogeneous molecular features.[1,2] The microsatellite stable and epithelial-to-mesenchymal transition (EMT) subtype of gastric cancer was reported as a molecular subtype in the Asian Cancer Research Group (ACRG) cohort.[2] The other subtypes include the microsatellite instability subtype,[1,2] the microsatellite stable subtype with or without *TP53* mutation,[2] and the Epstein-Barr virus subtype.[1] Approximately, 15%–30% of gastric tumors are classified as the EMT subtype.[2]

Because EMT has been found to underlie malignant tumor progression and therapeutic resistance, pharmacologic interventions against EMT pathways have garnered growing interest. However, directly targeting EMT-induced signaling pathways, for example, by inhibiting transforming growth factor-β, Wnt, and NOTCH,[3–5] has shown limited success, reflecting a narrow therapeutic window or lack of direct tumoricidal effect with these approaches.[6] Alternatively, synthetic lethal approaches, which attack indirect dependences associated with specific cancer biomarkers, could provide novel therapeutic options: a good example is a poly(adenosine diphosphatase–ribosyl)transferase-1 inhibitor, olaparib, approved by the US Food and Drug Administration, which has a synthetic lethal effect on ovarian tumors containing BRCA1 and 2 mutations.

In the present study, we sought to characterize the EMT status of 29 gastric cancer cell lines and screen for small molecule pharmacologic compounds that have selective toxicity against EMT-subtype gastric cancer cell lines. We further investigated the mechanisms of EMT selectivity and the in vivo efficacy of the nicotinamide phosphoribosyltransferase (NAMPT) inhibitor FK866 and the associations in protein expression between EMT markers and nicotinic acid phosphoribosyltransferase (NAPRT), a response biomarker to FK866, using gastric cancer tissues.

Methods

EMT Gene Signature Analysis

The EMT gene signature used in the present study was composed of 149 up- and 161 downregulated genes in gastric adenocarcinoma cohorts of the EMT subtype.[2] EMT-subtype

WHAT YOU NEED TO KNOW

BACKGROUND AND CONTEXT

Activation of epithelial–mesenchymal transition (EMT) in gastric cancer is associated with poor prognosis and therapy resistance. EMT selective therapeutic agents with direct tumoricidal effects are largely unknown.

NEW FINDINGS

Due to NAPRT deficiency, the NAMPT inhibitor FK866 is toxic to gastric cancer cells and tumor xenografts carrying markers of EMT activation. Expression of NAPRT is positively correlated with E-cadherin in primary and LNM gastric tumors.

LIMITATIONS

Sampling bias and small sample size prevented validation of NAPRT deficiency in relation to EMT in distant metastatic gastric tumors. Molecular mechanisms of EMT regulation by NAPRT need further study.

IMPACT

NAMPT inhibition could be a novel therapeutic strategy for EMT-subtype gastric cancer. NAPRT suppression in association with EMT is observed in several other tumor types, suggesting broad clinical implications beyond gastric cancer.

cell lines were detected by using unsupervised hierarchical clustering with average linkage based on the Euclidean distance of the gene expression values. EMT signature scores were calculated by subtracting the average $\log_2$-scale expression value of the 161 downregulated genes from that of the 149 upregulated genes. Tumor samples displaying significantly high EMT signature scores were detected from a *q-q* plot for each of the 31 datasets.

Gastric Tumor Subjects and Tissue Microarray Analysis

The present study was approved by the institutional review board of Severance Hospital (Seoul, South Korea; 4-2015-0616, 4-2017-0978). Demographic and clinical information and tumor tissue samples were obtained from 942 patients with gastric cancer who had undergone curative-intent gastrectomy from 2000 through 2003 at Severance Hospital. Patient age, sex, tumor histology, Lauren classification, and pathologic TNM stages were evaluated as clinical parameters. The median follow-up time was 112 months (range, 1–163 months). Immunohistochemical analysis of sections of tissue microarray

Ⓐ Most current article

(TMA) blocks containing 942 gastric tumor tissue samples was performed using a Ventana XT Automated Stainer (Ventana Medical Systems, Tucson, AZ) and anti-NAPRT (NBP1-87243; Novus Biologicals, Littleton, CO), anti-vimentin (PA0033; Leica Biosystems, Buffalo Grove, IL), and anti–E-cadherin (E-CAD-L-CE; Leica Biosystems) antibodies. In addition, immunohisto-chemical analyses of a commercial TMA (Pantomics, Richmond, CA) containing 48 matched primary and lymph node metastatic gastric tumor tissue samples and 33 matched primary and distant metastatic gastric tumor tissue samples (Severance Hospital) were performed using the same antibodies. For statistical analysis, intergroup comparison was conducted using a χ^2 test for each of the clinicopathologic variables. Student t test was used for age. A P value less than .05 was considered statistically significant. All statistical tests were 2-sided prob-ability tests. All statistical analyses were conducted in the R language environment (http://www.r-project.org).

Tumor Xenograft Studies

The construction of the gastric tumor xenograft model was approved by the institutional review board of Severance Hospital (4-2013-0526), and all patients provided written informed consent. The studies of preclinical FK866 treatment were approved by the institutional animal care and use com-mittee of the Yonsei University College of Medicine (Seoul, South Korea; 2014-0130). Before the experiments, the animals were acclimated for 7 days with 12-hour light and dark cycles. A surgically dissected tumor from a relevant patient was implanted into a subcutaneous area in the right flanks of BALB/c-nude mice (subsequently called F1 mice). When the tumor in the F1 mouse grew to a volume of 500 mm^3, it was removed for serial transplantation to the next generations of mice (F2 and F3). The established xenograft tumors were expanded in vivo using BALB/c nude mice. When tumor volumes reached approximately $100 \sim 200$ mm^3, the animals were randomized into 2 groups for treatment. Mice with GA077 tumors were injected intraperitoneally with FK866 20 mg/kg (n = 5) or with vehicle (48% propylene glycol and 3% β-hydro-cyclodextrin; n = 6) twice daily for 24 days. Tumor volume was determined in a blinded manner through caliper measurements 3 times per week according to the formula, (length $\times$ width^2)/2. After treatment completion, the mice were anesthetized with Zoletil (tiletamine and zolazepam; Virbac, Carros, France) and Rompun (xylazine; Bayer Healthcare, Berlin, Germany; 6:4). The tumors were surgically removed, weighed, minced into small pieces, and stored at $-80°C$ until further analysis.

Results

Gastric Cancer Cell Lines Mirror the Molecular Subtypes Observed in Primary Tumors

To identify a set of gastric cancer cell lines exhibiting molecular signatures and behaviors representative of the EMT subtype, we assembled a panel of 29 DNA-fingerprinted gastric cancer cell lines (Figure 1A and Supplementary Table 1). Because the EMT signature has been found to be highly correlated with the first principal component in the ACRG cohort,[2] we performed an unsuper-vised hierarchical clustering analysis of EMT signature genes with RNA-seq fragments per kilobase per million mapped

reads for the gastric cancer cell lines (Supplementary Data 1A). Using the EMT signature (Supplementary Data 1B), we classified 26 of the 29 gastric cancer cell lines into the mesenchymal (n = 7) or epithelial (n = 19) subtype (Figure 1B). To exclude the possibility of sampling bias that could exist in non–EMT-subtype gastric cancer cell lines, non-EMT cell lines were further classified into 4 additional molecular subtypes. The microsatellite instability subtype was identified based on the increased mutation burden (Figure 1C), allelic shift of 5 mononucleotide microsatellite markers (Supplementary Table 2), and low expression of the *MLH1* DNA repair gene (Figure 1D). The Epstein-Barr virus subtype was identified based on the detection of Epstein-Barr virus sequences using DNA and mRNA analyses (Supplementary Table 3), and the microsatellite stable sub-type was categorized with or without the *TP53* mutation. We found that 22 non-EMT cell lines covered all 4 non-EMT gastric cancer subtypes observed in primary tumors. Notably, the expression of *VIM* and *CDH1*, 2 reference marker genes for the EMT signature, was sufficient to discriminate EMT cell lines from non-EMT cell lines (Figure 1D). To further confirm that these cell lines mirrored the genetic features observed in primary gastric tumors,[1,2] we assessed consistencies in frequently mutated genes (Figure 1C) and commonly occurring copy number variations (Supplementary Figure 1 and Supplementary Data 1C–E) and found that these cell lines showed very similar patterns in mutational and copy number profiles compared with primary tumors. These data supported that the 29 cell lines tested accurately and reflected clinical subtypes of gastric cancer. Thus, all 29 cell lines were subjected to further analyses.

EMT-Subtype Gastric Cancer Cells Are Hypersensitive to Inhibition of NAMPT

To confirm the mesenchymal properties of the 7 gastric cancer cell lines identified as being of the EMT subtype (Hs746T, SNU1750, MKN1, SK4, SNU484, SNU668, and YCC11), we assessed the steady-state accumulation of EMT markers and the physiologic ability of the cells to invade extracellular matrices. In agreement with the gene expres-sion data, the EMT-subtype gastric cancer cell lines tended to exhibit increased expression of mesenchymal proteins (vimentin and fibronectin) and EMT-driving transcription factors (ZEB1 and Snail) and the depletion of epithelial proteins (E-cadherin, EpCAM, and claudin-7) and the epithelial transcription factor GRHL2 compared with non-EMT cell lines (Figure 2A). Moreover, EMT cell lines demonstrated a significantly greater capacity to invade Matrigel-coated Transwell membranes compared with non-EMT cell lines ($P = .026$ by Wilcoxon rank sum test; Supplementary Figure 2A).

The induction of EMT often results in the acquisition of stem cell–like properties.[7] Therefore, we tested whether the selected gastric cancer cell lines expressed the CD44 stem cell marker and had the ability to form tumor spheres. Indeed, 5 of the 7 EMT-subtype gastric cancer cell lines expressed CD44 (Figure 2A), and all EMT-subtype gastric cancer cell lines formed significantly larger numbers of

A

B

C

D
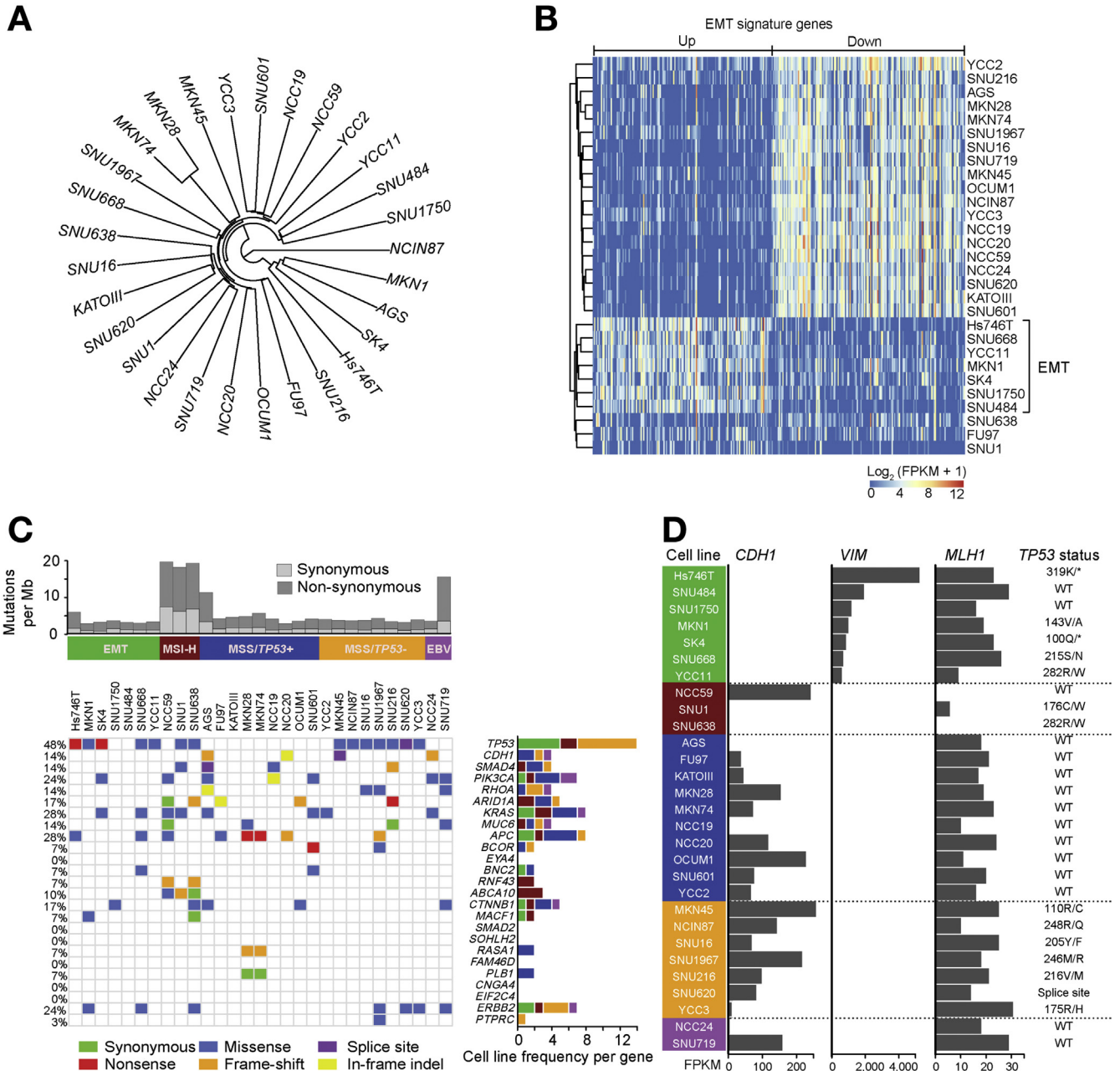
Figure 1. Molecular classification identifies EMT-subtype gastric cancer cell lines. (*A*) Cell line ontology of the 29 gastric cancer cell lines. (*B*) Classification of the 29 gastric cancer cell lines according to their EMT gene expression signatures. Columns represent genes belonging to the EMT signature (149 upregulated genes on the left, 161 downregulated genes on the right). (*C*) Somatic mutation frequency and mutation types for the 29 gastric cancer cell lines. The color-coded matrix in the central panel indicates individual mutation types in the 29 gastric cancer cell lines for 25 previously reported, significantly mutated genes that have a higher mutation rate than the background mutation rate in the primary gastric tumor (n = 215), rank ordered based on q values.[1] The percentage of cell lines carrying a mutation per gene is represented on the left side of the matrix. Subtype selective mutation frequencies for each of the 25 genes are represented in the right panel. (*D*) Summary of cell line classification, showing cell line characteristics for the representative features relevant to each molecular subtype. The expression levels (FPKM) of *CDH1* (E-cadherin), *VIM* (vimentin), and *MLH1* are represented as *horizontal bars*. EBV, Epstein-Barr virus; FPKM, fragments per kilobase per million mapped reads; MSI, microsatellite instability; MSS, microsatellite stable; WT, wild type.

tumor spheres under nonadherent conditions in the serum-free medium, although the numbers, sizes, and appearances thereof varied among cell lines (*P* = .02 by Wilcoxon rank sum test; Supplementary Figure 2*B*).

Next, we subjected the EMT gastric cancer cell lines to a single-concentration (2.5 μmol/L) primary drug screen

encompassing 1,345 pharmaceutical compounds (1,132 drugs approved by the US Food and Drug Administration and 213 anticancer compounds; Supplementary Data 2*A*). Sixty-three compounds induced a greater than 50% decrease in cell viability in at least 4 of the 7 tested EMT gastric cancer cell lines after 72 hours of exposure

(Supplementary Figure 2C). Secondary screens were subsequently performed by treating all 29 gastric cancer cell lines in duplicate with the 63 compounds, which were prepared in 12-point half-log serial dilutions. Cell line–specific responses to each of the 63 compounds were assessed by estimating the mean areas under the viability curve (Supplementary Figure 2D and Supplementary Data 2B). Fourteen compounds exhibited selective toxicity against the EMT gastric cancer cell lines with a false discovery rate lower than 10% by a median difference greater than 1 in the area under the viability curve (Figure 2B).

Remarkably, treatment with FK866, a highly potent and competitive NAMPT inhibitor,[8–10] induced a clear bimodal response: 6 of the 7 EMT gastric cancer cell lines showed hypersensitivity to the drug (false discovery rate, 5.189%; $P = .01339$ by Student t test), with the median lethal dose in the nanomolar range (Figure 2C). In resistant cell lines, most of which were non-EMT cell lines, the drug was nontoxic up to the highest testable concentration (50 μmol/L), thus reflecting a greater than 1,000-fold selectivity. The bimodality implies that the drug response is determined by a single underlying factor. Therefore, FK866 was selected for further investigation.

To assess the in vivo efficacy of FK866, we chose an EMT-activated tumor model from our collection of well-characterized gastric tumor xenograft models.[11] This EMT-subtype tumor, a poorly differentiated adenocarcinoma (GA077), expressed lower levels of NAPRT and E-cadherin and higher levels of vimentin and active forms of SMAD2 and 3 than a matched normal sample (Figure 2D). Tumor regression was observed after 2 weeks of FK866 treatment (Figure 2E). The difference between GA077 tumor growth curves for FK866-treated and vehicle-treated mice was statistically significant in an analysis of variation treatment-by-time interaction analysis ($P = 1.9 \times 10^{-5}$). After treatment completion, tumors in the FK866-treated mice exhibited a 5-fold decrease in tumor volume and a 3-fold decrease in tumor weight compared with mice treated with vehicle alone (Figure 2E and Supplementary Figure 3A). In contrast, a xenograft of the MKN45 non-EMT gastric cancer cell line did not respond to FK866, even at a higher treatment dose (25 mg/kg; Supplementary Figure 3B–D). The body weight and food intake of the FK866- and vehicle-treated animals remained similar (Supplementary Figure 3E), suggesting there was no treatment-related toxicity. In addition, no decrease in platelet count was observed at the tested doses (20 and 25 mg/kg) of FK866 (Supplementary Figure 3F), although thrombocytopenia has been reported as a major adverse event in phase I clinical trials of FK866 and other NAMPT inhibitors.[12]

Intrinsic Loss of NAPRT Expression in EMT-Subtype Cancers Elicits Synthetic Lethality to NAMPT Inhibition

Next, we sought to determine the mechanism by which the NAMPT inhibitor FK866 exerted its effects on EMT gastric cancer cell lines. By converting nicotinamide to nicotinamide mononucleotide, NAMPT mediates a salvage pathway for synthesizing nicotinamide adenine dinucleotide (NAD$^+$), a coenzyme crucial to sustaining cellular energy and redox homeostasis in all living cells.[8,10] In addition, as an alternative salvage pathway, NAPRT uses nicotinic acid as a substrate for synthesizing NAD$^+$. In some cancer contexts, loss of NAPRT has been observed to facilitate synthetic lethality to inhibition of NAMPT.[10,13,14] Therefore, we hypothesized that the hypersensitivity to FK866 that we observed in the EMT gastric cancer cell lines might reflect NAPRT deficiency. To test this, we measured steady-state protein levels of NAPRT in the 7 EMT gastric cancer cell lines and the 7 randomly selected non-EMT FK866-resistant gastric cancer cell lines. Depletion of NAPRT was observed in 5 of the 7 EMT cell lines (Figure 3A). Furthermore, we observed that NAPRT protein levels were correlated with the EMT cell line–associated sensitivity to FK866 reported earlier. For example, SK4, which expressed normal levels of NAPRT (Figure 3A), showed resistance to FK866 (Figure 2C). YCC11, which expressed lower levels of NAPRT than the other non-EMT cell lines (Figure 3A), exhibited moderate sensitivity to FK866 (Figure 2C). In addition, 5 of the 7 non-EMT cell lines (MKN28, MKN74, FU97, NCC19, and SNU16) that displayed exceptional hypersensitivity to FK866 showed NAPRT deficiency (Supplementary Figure 4A).

Moreover, gastric cancer cell lines that expressed normal levels of NAPRT, irrespective of their EMT status, were sensitized to FK866 after depletion of NAPRT with small interfering RNA (Figure 3B), indicating that the depletion of NAPRT expression is sufficient to confer FK866 hypersensitivity. Consistent with the canonical function of NAPRT and NAMPT, treatment of NAPRT-deficient EMT gastric cancer cell lines with FK866 for 40 hours resulted in significant decreases in NAD levels (Figure 3C). Treatment of the NAPRT-positive non-EMT gastric cancer cells did not affect NAD levels (Figure 3C).

To determine whether the observed therapeutic effect of FK866 in the GA077 tumor xenograft was mediated by NAD depletion, an on-target effect, we measured total NAD levels from the harvested tissues after treatment completion. Indeed, NAD levels were decreased by 78% in tumors treated with FK866 compared with those treated with vehicle alone ($P = 5.7 \times 10^{-5}$ by Student t test; Figure 3D). These results suggested decreased NAD levels might be the cause of the observed toxicity in EMT gastric cancer cells. In addition, the expression of NAPRT remained suppressed in the F3 generation of GA077 tumors in the FK866- and vehicle-treated conditions (Figures 3E and 3F); this is important because reversal of a target biomarker is a common mechanism of acquired anticancer drug resistance. These data suggested that downregulation of NAPRT could occur through an irreversible mechanism in the GA077 model.

We further validated these findings by showing that overexpression of NAPRT in NAPRT-deficient EMT cell lines almost completely reversed toxicity to FK866 (Figure 3G). Similarly, cotreatment with NAD or nicotinamide reversed the observed toxicity to FK866 in a dose-dependent manner, whereas nicotinic acid did not have this effect (Supplementary Figure 4B). These observations indicated that most EMT gastric cancer cell lines tested were extremely

A

B
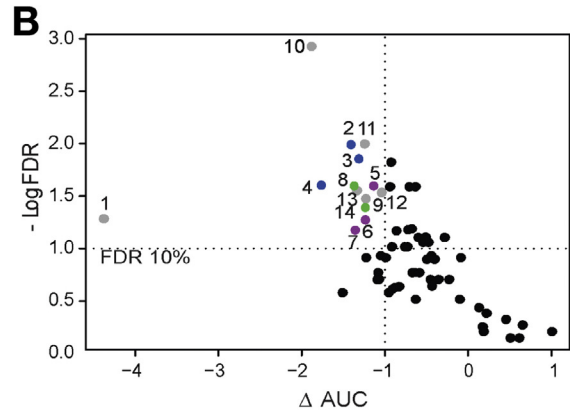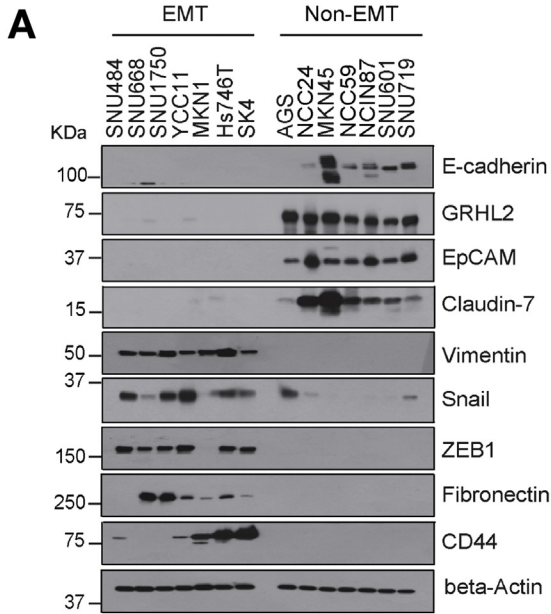
1. FK866
2. Doxorubicin (Adriamycin)
3. Mitoxantrone Hydrochloride   Topoisomerase II inhibitor
4. Daunirubicin HCl
5. Torin2
6. INK128   mTOR/PI3K inhibitor
7. BEZ235 (NVP-BEZ235)
8. Vincristine
9. Vinblastine   Microtubule destabilizer
10. YM155
11. Ouabain
12. Niclosamide
13. Terfenadine
14. Obatoclax mesylate (GX15-070)

C

D

E

$P = 1.9 \times 10^{-5}$
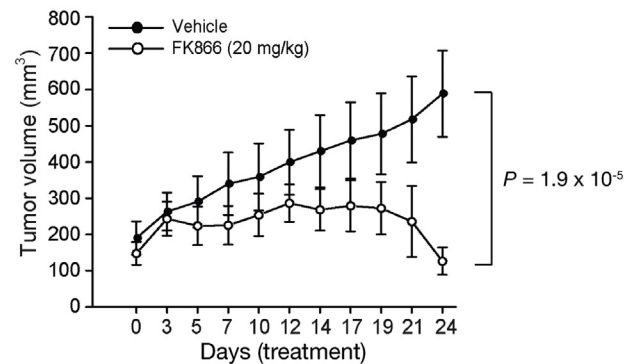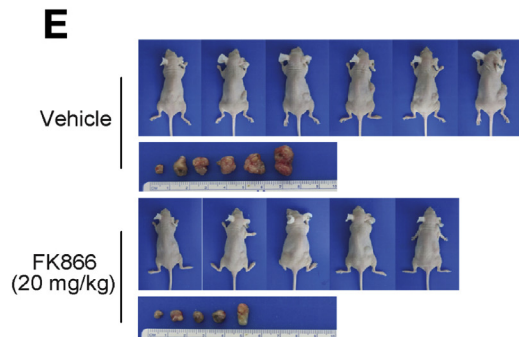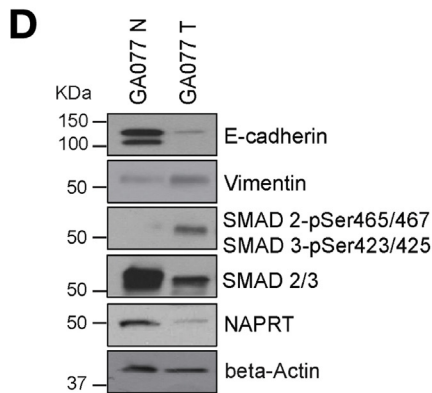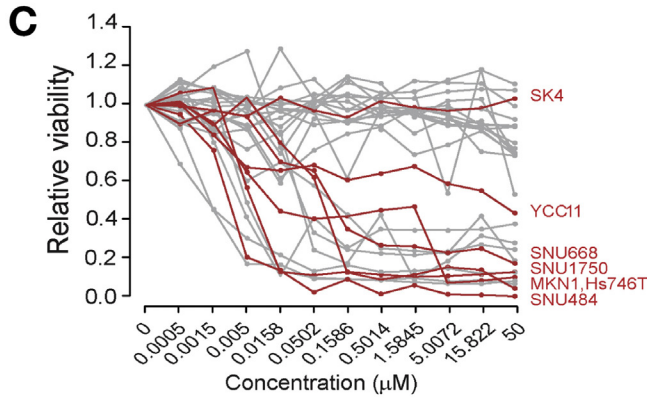
vulnerable to inhibition of NAMPT, suggesting that FK866 exerts its effects on these cells through the synthetic lethality of NAMPT inhibition with NAPRT deficiency.

EMT-Associated Downregulation of NAPRT Is Observed in Primary and Metastatic Gastric Tumors

To confirm our cell line–based discoveries of EMT-associated suppression of NAPRT expression in primary tumors, we compared *NAPRT* expression levels between EMT and non-EMT gastric tumor samples. EMT-subtype gastric tumors in the ACRG cohort[2] (N = 300, $P = 3.4 \times 10^{-15}$ by Student t test), The Cancer Genome Atlas (TCGA) cohort[1] (N = 375, $P = 1.4 \times 10^{-10}$ by Student t test), and the Singapore cohort[15] (N = 200, $P = 2.2 \times 10^{-13}$ by Student t test) expressed significantly lower levels of *NAPRT* (Supplementary Figure 5 and Figure 4A), whereas normal samples available in the TCGA cohort expressed *NAPRT* at levels similar to those in non-EMT tumors.

We further investigated whether NAPRT protein expression correlated with clinicopathologic parameters in samples from patients with gastric cancer (942 TMA samples, 178 of which had gene expression microarray data). Although patient sex and TNM stage were similar in patients with NAPRT-negative (n = 402) and NAPRT-positive (n = 540) gastric cancer, age ($P = .019$ by Student t test), histology ($P < .001$ by χ^2 test), and Lauren subtype ($P < .001$ by χ^2 test) displayed statistically significant differences between the 2 groups (Table 1). These differences are attributable to EMT status. Previously, the ACRG reported that 80.4% of subjects with a tumor of the EMT subtype were diagnosed with diffuse-type cancers ($P < .0001$) and at a significantly younger age ($P = .03$) than those with non-EMT subtypes.[2] In support of these observations, 178 TMA samples exhibited strong associations between EMT subtype and depletion of NAPRT at the mRNA level ($P = .000001$ by Wilcoxon rank sum test; Supplementary Figure 6B) and the protein level ($P = .000122$ by Fisher exact test; Supplementary Figure 6C). In support of this finding, we noted a strong positive correlation between E-cadherin and NAPRT levels in all 942 TMA samples ($P < .001$ by χ^2 test; Table 1). As shown in Figure 4B, strong expression of NAPRT (mainly in the cytoplasm) and E-cadherin (mainly in the membrane) was observed in moderately differentiated adenocarcinoma (intestinal subtype), whereas complete loss of NAPRT and

E-cadherin was observed in signet ring cell carcinoma (diffuse subtype).

Notably, marked differences were discovered in the frequencies of EMT-subtype tissues expressing a gene expression signature (26%; Supplemental Figure 6A) and E-cadherin negativity (8.4%; Table 1). This might suggest that some samples positive for E-cadherin listed in Table 1, particularly those with weak E-cadherin positivity, include samples of the EMT subtype. In support of this possibility, when only E-cadherin positive tumors were considered, NAPRT negativity remained significantly associated with weak E-cadherin positivity ($P = .0002$ by Fisher exact test). Surprisingly, when only the 131 non-EMT samples from the 178 tumor samples with microarray data were considered, a statistically meaningful positive correlation was still identified between *NAPRT* and *CDH1* (Supplementary Figure 6D). These results suggest that downregulation of NAPRT also might occur in some non-EMT gastric tumors of partial EMT status.

This positive correlation between E-cadherin and NAPRT was reproduced in an orthogonal TMA panel containing 48 matched primary and lymph node metastatic gastric tumor samples ($P = .00006$ in primary samples and $P = .016$ in lymph node metastasis samples by Pearson correlation test; Supplementary Table 4). In addition, although there was unexpected heavy sampling bias toward non-EMT tumors, 5 of 33 matched distant metastatic gastric tumor samples (Supplementary Table 5) displayed metastatic co-depletion of E-cadherin and NAPRT (n = 3; Supplementary Figure 6E) or NAPRT negativity independent of E-cadherin status (n = 2; Supplementary Figure 6F). Our analyses of clinicopathologic parameters and immunohistologic data suggested that NAPRT expression is frequently lost in EMT-subtype gastric cancer and could represent a reliable and legitimate biomarker for patient selection for treatment with NAMPT inhibitors.

## EMT-Associated Downregulation of NAPRT Is Conserved in Different Tumor Types

To investigate whether EMT-subtype–associated downregulation of *NAPRT* is present in cancer types other than gastric cancer, we carried out a meta-analysis of 31 publicly available, large-scale gene expression datasets (sample size > 100) from 17 major tumor types. Twelve of the 17 tumor types had at least 1 dataset (from 21 datasets in total) that

Figure 2. EMT-subtype gastric cancer cells are hypersensitive to inhibition of nicotinamide phosphoribosyltransferase. (*A*) Steady-state accumulation of the indicated proteins was assessed by western blotting of whole cell lysates from the indicated EMT and non-EMT gastric cancer cell lines. β-Actin was used as a loading control. (*B*) Identification of EMT-subtype selective pharmacologic compounds. Cell line–specific responses to 63 compounds were used to calculate ΔAUC, the median differences of AUC between EMT and non-EMT gastric cancer cell lines (*x*-axis). FDR values (*y*-axis, in negative log scale) were obtained using the Benjamini-Hochberg correction of P values derived by Student t test. (*C*) Dose-response curves of cell viability for 29 gastric cancer cell lines after 72 hours of exposure to FK866. The 7 gastric cancer cell lines of EMT subtype are indicated in *red*. (*D*) Steady-state accumulation of EMT marker proteins. Protein levels were assessed by immunoblotting of GA077 patient tumor (*T*) and patient normal (*N*) samples. (*E*) Efficacy of FK866 in xenograft tumors. The mice were imaged before being sacrificed and the tumor volumes were measured on the indicated days. Treatment-by-time interaction P values by analysis of variance are shown. Error bars indicate ±SEM (n = 6). AUC, area under viability curve; FDR, false discovery rate.
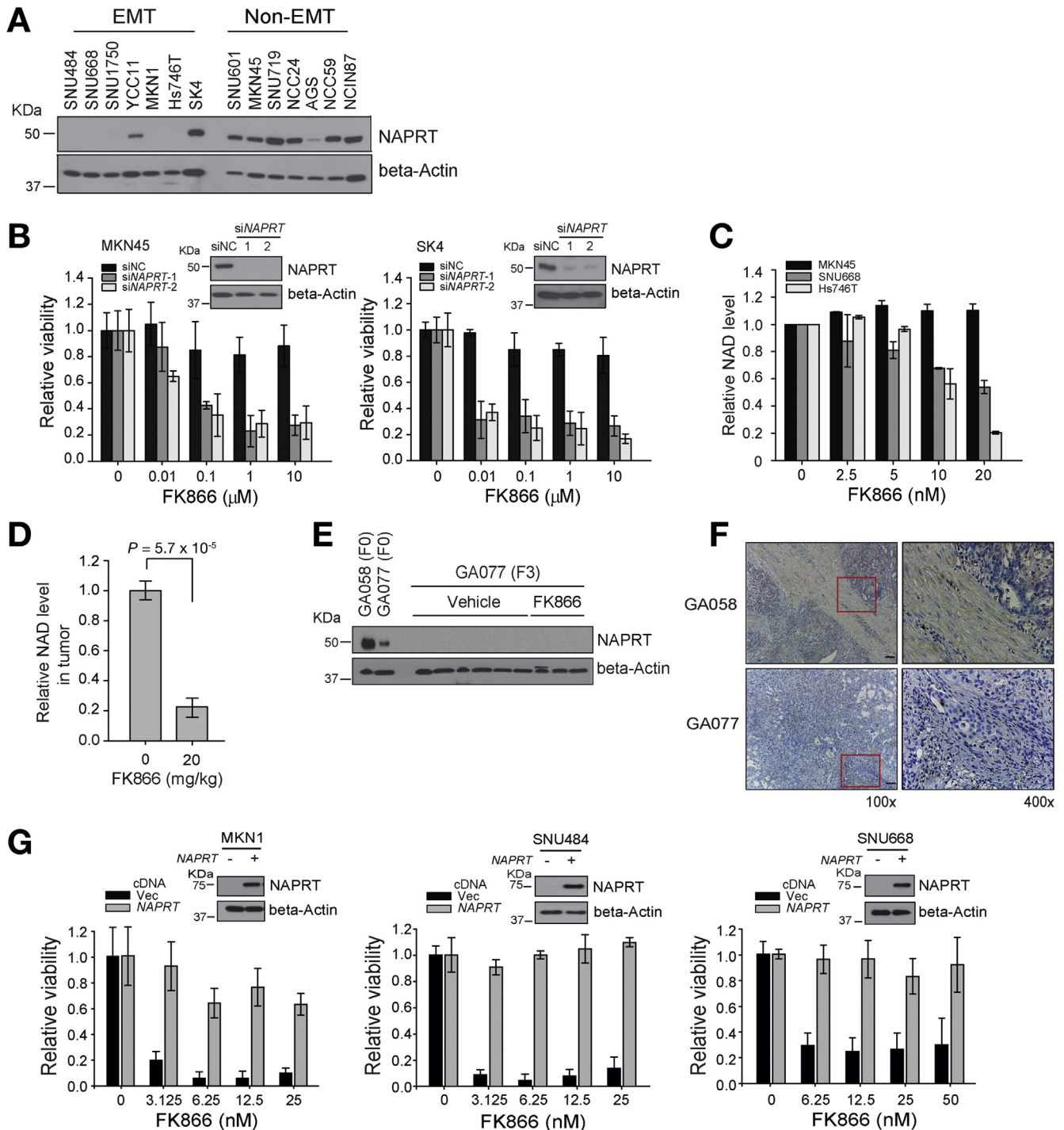
Figure 3. Suppression of NAPRT expression in EMT-subtype gastric cancer cell lines generates synthetic lethality to NAMPT inhibition. (*A*) Steady-state accumulation of NAPRT was assessed by immunoblotting of whole cell lysates from the indicated EMT and non-EMT gastric cancer cell lines. (*B*) The indicated siRNAs were tested to evaluate their effects on FK866-dependent toxicity in MKN45 and SK4 cells. (*Insets*) Immunoblotting was performed to confirm NAPRT depletion. Error bars indicate ±SD (n = 3). The siNC is the negative control siRNA, and siNAPRT-1 and 2 are 2 different siRNA oligos targeting NAPRT. (*C*) Total NAD levels measured in EMT-subtype (SNU668 and Hs746T) or non–EMT-subtype (MKN45) gastric cancer cell lines after exposure to the indicated concentrations of FK866. Error bars indicate ±SD (n = 3). (*D*) Relative NAD levels to total protein levels in GA077 tumors after 24 days of treatment with FK866 (20 mg/kg) or vehicle. Error bars indicate ±SD (n = 6). (*E*) Steady-state accumulation of NAPRT in patient tumor and tumor xenograft specimens (GA077, F3 generation) treated with injections of vehicle (n = 6) or FK866 (20 mg/kg; n = 3) lysates. GA058 (F0 primary tumor) was used as a control to represent a non-EMT tumor. (*F*) NAPRT expression was detected in the indicated non-EMT (GA058, F0) and EMT (GA077, F3) tumor specimens by immunohistochemistry. *Scale bars* represent 100 μm. (*G*) The indicated cDNAs were tested to evaluate their effects on FK866-dependent toxicity in the EMT-subtype cells. (*Insets*) Immunoblots confirm ectopic expression of NAPRT (with green fluorescent protein tag). *Error bars* indicate ± SD (n = 3). siRNA; small interfering RNA; Vec, empty vector.
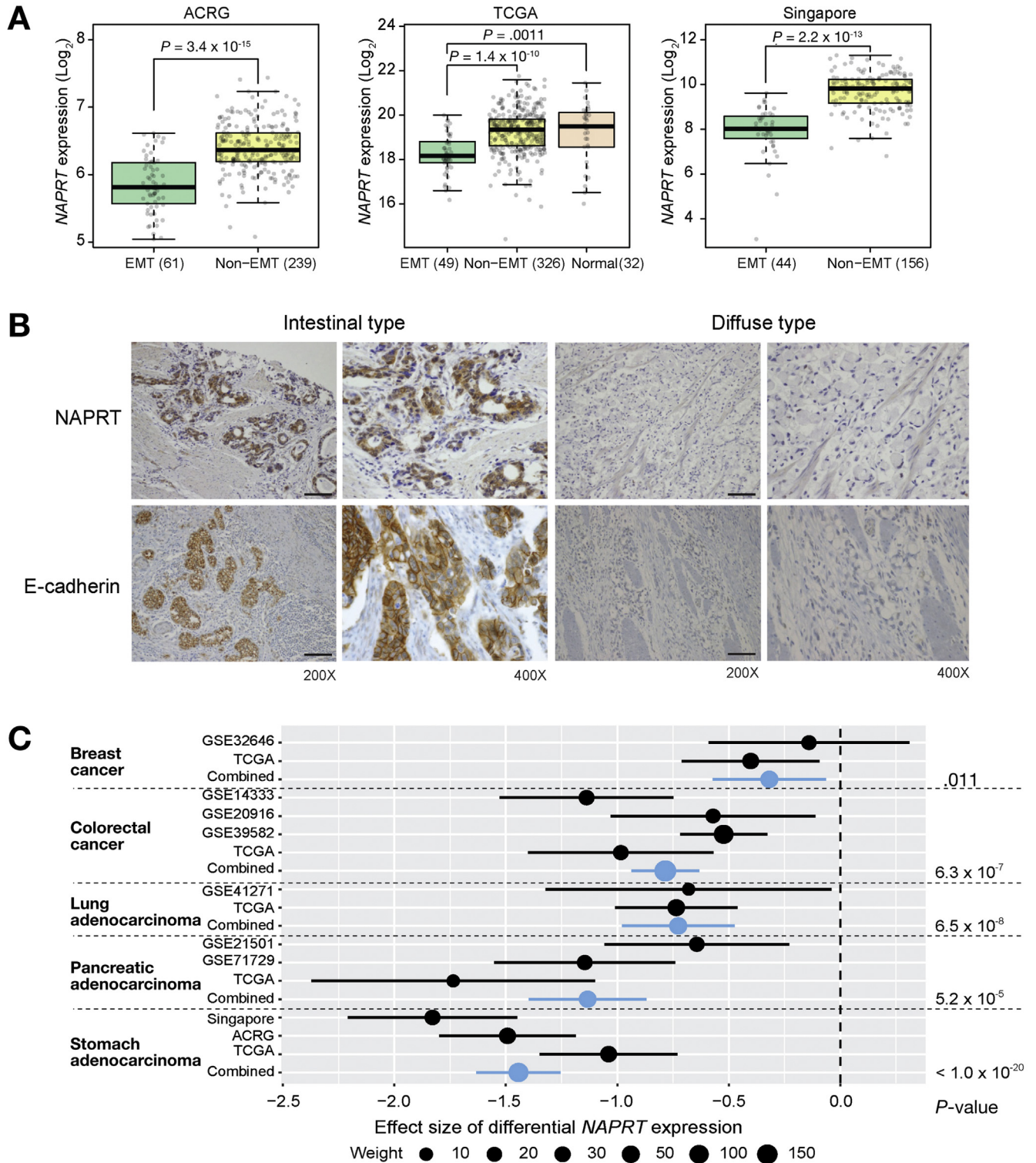
Figure 4. EMT-associated suppression of NAPRT is observed at the mRNA and protein levels and is conserved in different tumor types. (*A*) Comparison of *NAPRT* expression levels in EMT and non-EMT tumor samples. The group sizes for each cohort are shown in parentheses. *P* values by Student *t* test are displayed for the comparisons between EMT and non-EMT tumor samples and between EMT tumor and normal samples, respectively. Box-and-whisker plots represent the median (*middle line*), first quartile (*lower bound line*), third quartile (*upper bound line*), and the ±1.5 interquartile range (*whisker lines*), with raw data overlaid. (*B*) Representative images of immunohistochemistry staining of NAPRT and E-cadherin in the cohort of gastric tissue microarray specimens. See Table 1 for a formal statistical analysis (N = 942). *Scale bars* represent 100 *μ*m. (*C*) Forest plots display study-specific (*black*) and overall (*blue*) effect sizes (*filled circles*) and 95% CIs (*horizontal bars*) of the differential NAPRT expression between EMT and non-EMT tumor samples. The sizes of the circles are proportional to the weight assigned to each study, as estimated by a random-effects model. The permutation-based *P* value for the overall effect is shown for each tumor type.

Table 1. Expression of NAPRT and Clinicopathologic Characteristics of 942 Patients With Gastric Cancer

	Overall	NAPRT negative (n = 402)	NAPRT positive (n = 540)	P value by χ^2 test
Age (y)	57.2 ± 12.02	56.21 ± 12.65	58.10 ± 11.47	.019[a]
Sex				.153
Male	617	253 (41%)	364 (59%)	
Female	325	149 (46%)	176 (54%)	
Histology				<.001
Differentiated	280	74 (26%)	206 (74%)	
Undifferentiated	662	328 (50%)	334 (50%)	
Lauren classification				<.001
Intestinal	461	151 (33%)	310 (67%)	
Diffuse	411	226 (55%)	185 (45%)	
Mixed	70	25 (37%)	45 (63%)	
pT stage				.423
pT1	3	2 (67%)	1 (33%)	
pT2	157	74 (47%)	83 (53%)	
pT3	134	50 (37%)	84 (63%)	
pT4	648	276 (43%)	372 (57%)	
pN stage				.310
pN0	257	120 (47%)	137 (53%)	
pN1	177	76 (43%)	101 (57%)	
pN2	182	79 (43%)	103 (57%)	
pN3	326	127 (39%)	199 (61%)	
TNM stage				.140
I	96	46 (48%)	50 (52%)	
II	243	113 (47%)	130 (53%)	
III	603	243 (40%)	360 (60%)	
E-cadherin				<.001
Negative[b]	79	56 (71%)	23 (29%)	
Weak positivity	354	168 (47%)	186 (53%)	
Strong positivity	480	166 (35%)	314 (65%)	
NA	29			

NA, not available; pN, regional lymph nodes; pT, primary tumor.
[a]By Student t test.
[b]Complete loss of expression on the membrane.

showed expression of the EMT signature in more than 3% of samples (Supplementary Data 3). In 20 of the 21 examined datasets for these 12 tumor types, samples of the EMT subtype displayed lower average *NAPRT* expression than non-EMT samples, and in 8 tumor types (bladder urothelial carcinoma, breast cancer, colorectal cancer, head and neck squamous cell carcinoma, kidney renal papillary cell carcinoma, lung adenocarcinoma, pancreatic ductal adenocarcinoma, and stomach adenocarcinoma), EMT-subtype samples had significantly lower levels of *NAPRT* expression than non-EMT samples ($P < .01$ by Student test; Supplementary Figures 7A, 7B and Supplementary Data 3). Notably, 5 of the 8 tumor types were represented by data from at least 2 cohorts. Of these tumor types, stomach adenocarcinoma exhibited the largest effect sizes (unbiased standardized mean difference in *NAPRT* expression, −1.44) with extremely low permutation test *P* values ($<10^{-20}$; Figure 4C and Supplementary Data 3). Taken together, these results suggest that EMT-associated downregulation of *NAPRT* is conserved in different tumor types and that the EMT subtypes of gastric cancer might be high-priority candidates for potential treatment with NAMPT inhibitors.

Promoter Hypermethylation Is Associated With Downregulation or Aberrant Transcription of NAPRT

Promoter hypermethylation is a well-known mechanism of gene silencing in cancer.[16] Previous studies have reported that *NAPRT* promoter hypermethylation at CpG islands is commonly found in cancer cell lines lacking *NAPRT* expression.[14,17] In agreement with previous reports, complete (MKN1, SNU484, and SNU668) or partial (YCC11 and Hs746T) *NAPRT* promoter methylation was observed in EMT gastric cancer cell lines in which NAPRT was not detected (Figure 5A). Notably, the SNU484 and MKN1 cell lines expressed aberrant *NAPRT* transcripts lacking the first exon. These results suggest that the aberrant transcription might have occurred through the use of an alternative transcription start site as a consequence of promoter hypermethylation (Figure 5B). Loss of exon 1 can result in mRNA without a start codon, which would not be translated. However, no promoter methylation was detected in SK4 (which expresses normal levels of NAPRT) and SNU1750 EMT gastric cancer cell lines. Of interest, although SNU1750 had an unmethylated *NAPRT* promoter and expressed normal levels
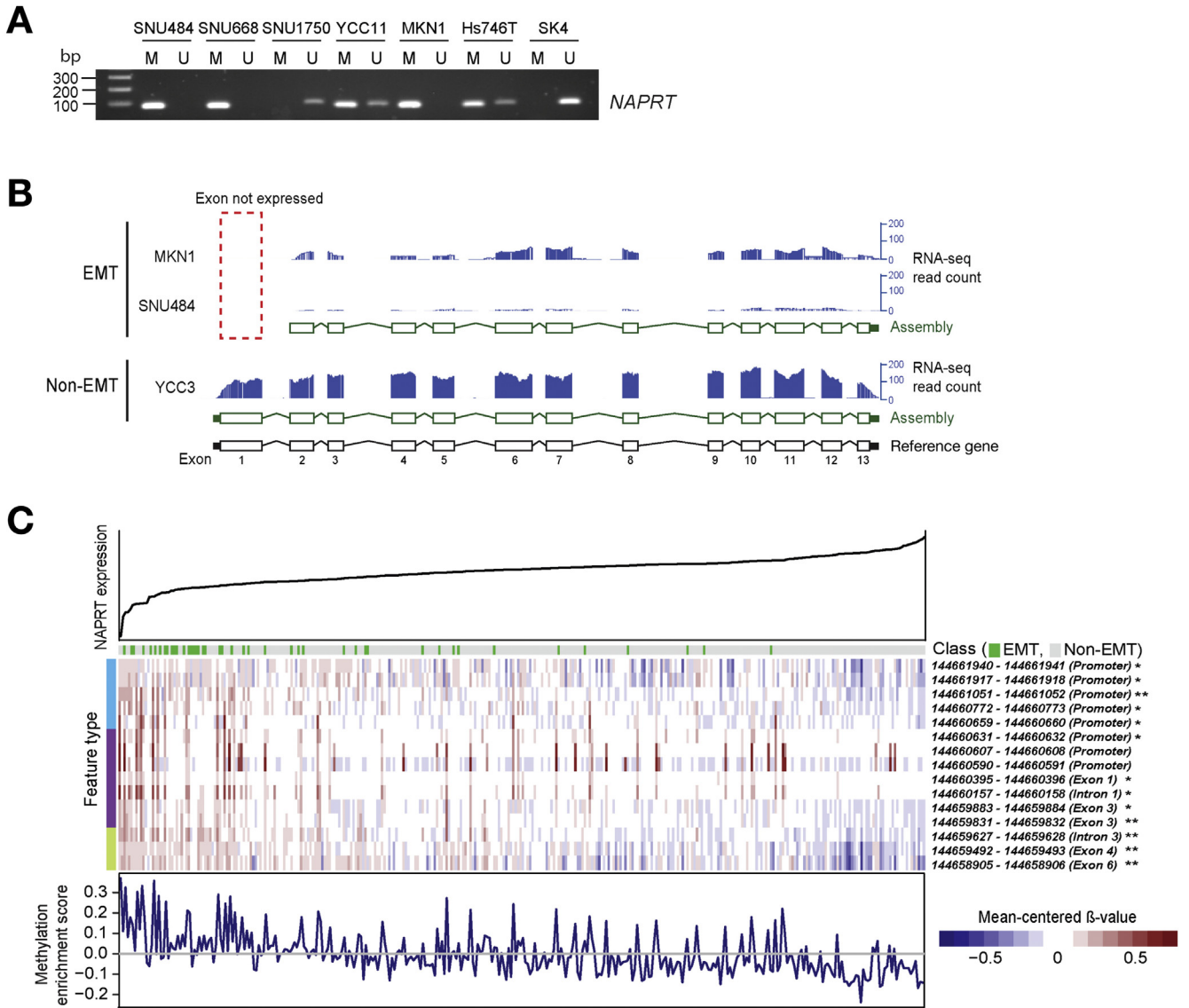
Figure 5. Promoter hypermethylation is associated with suppression of *NAPRT* expression or aberrant transcription of *NAPRT*. (*A*) Analysis of the methylation-specific polymerase chain reaction products of *NAPRT* promoter CpG islands in 7 EMT gastric cancer cell lines. (*B*) RNA-seq coverage plots for *NAPRT* transcripts from MKN1 and SNU484 (EMT subtype) and YCC3 (non-EMT subtype) generated with the Integrated Genome Browser.[31] (*C*) Correlation between *NAPRT* expression and *NAPRT* promoter CpG island hypermethylation in the TCGA stomach adenocarcinoma dataset. (*Upper panel*) *NAPRT* expression is displayed in ascending order for samples with transcriptome and methylation profiles (n = 338). (*Middle panel*) a heat map represents the mean-centered DNA methylation score for the CpG sites in the *NAPRT* promoter region. DNA site information on chromosome 8 is indicated on the right side of the heat map with the Pearson correlation test results between *NAPRT* expression and site-specific methylation score across the samples (*$P < 1.0 \times 10^{-8}$ and **$P < 1.0 \times 10^{-20}$). (*Lower panel*) Plot displays the cumulative methylation enrichment score representing more frequent promoter hypermethylation in the samples with lower *NAPRT* expression levels. M, polymerase chain reaction with methylation-specific primers; U, polymerase chain reaction with un-methylation–specific primers.

of *NAPRT* mRNA, it did not express NAPRT protein (Figure 3*A*), suggesting that additional post-transcriptional regulatory mechanisms beyond *NAPRT* promoter hypermethylation might operate in this cell line. A strong negative correlation also was observed between *NAPRT* expression levels and the methylation score of its promoter CpG island in the TCGA stomach adenocarcinoma datasets ($P < 1.0 \times 10^{-8}$ by Pearson correlation test; Figure 5*C*).

Together, these results suggest that *NAPRT* expression is potentially repressed in EMT-subtype gastric cancer by at

least 1 epigenetic and post-transcriptional mechanism, including promoter hypermethylation-mediated gene silencing or aberrant transcription.

Loss of NAPRT Expression Is Causally Linked to EMT Through Activation of Wnt/β-Catenin Signaling

Because *NAPRT* expression is downregulated in a wide variety of EMT tumors, we speculated that this
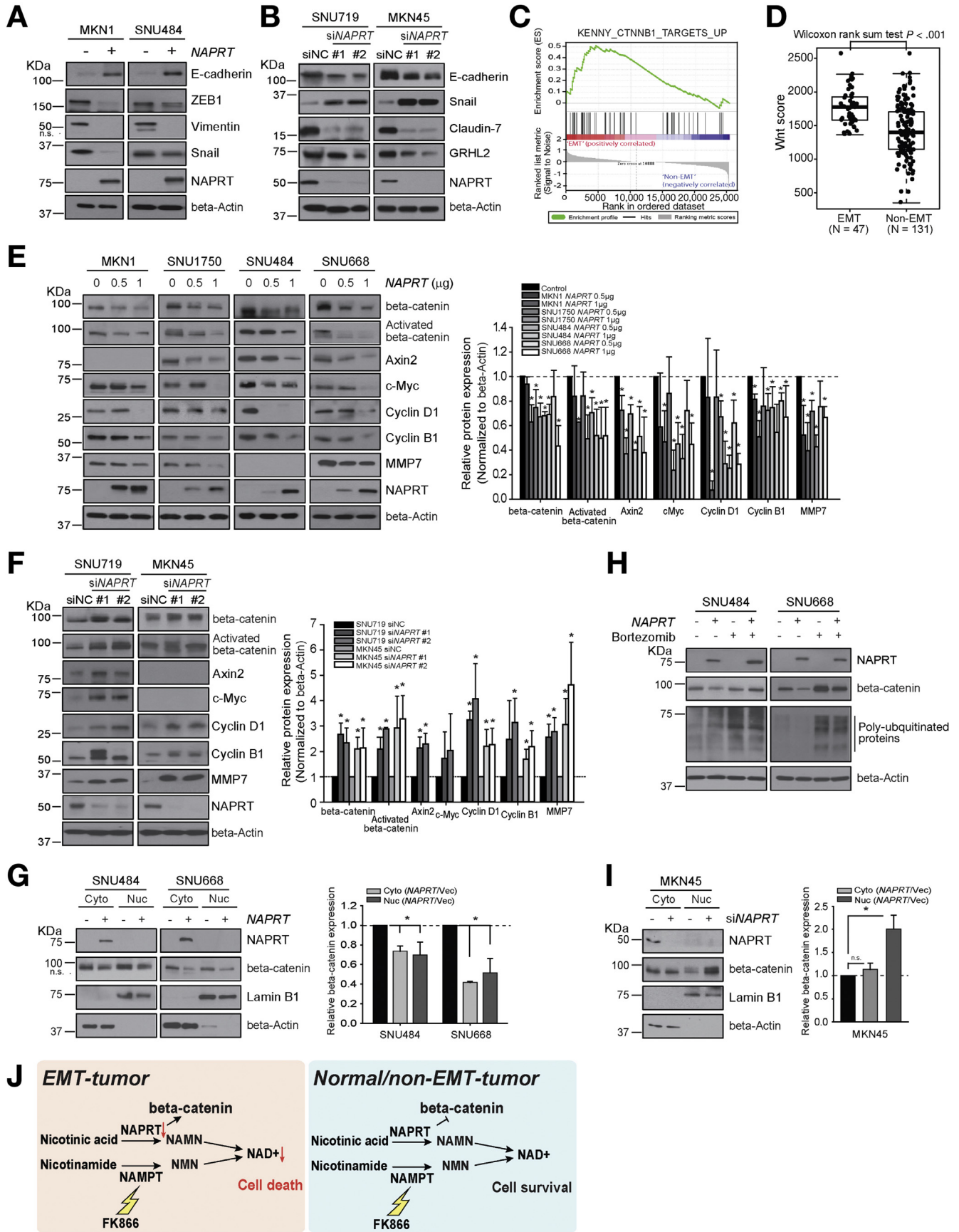
downregulation might be a cause of, rather than a consequence of, the EMT. In support of this hypothesis, we found that single-gene overexpression of *NAPRT* in EMT-subtype gastric cancer cells or knockdown in non-EMT–subtype gastric cancer cells was sufficient to reverse the expression of key EMT marker proteins characteristic of each subtype (Figures 6*A* and 6*B*). These data indicated that NAPRT is necessary to and sufficient for suppression of EMT. Interestingly, however, expression of vimentin, an end-stage EMT marker,[18] remained silenced at a single gene knockdown of *NAPRT* in non-EMT gastric cancer cells (data not shown), suggesting that other EMT factor(s) uncoupled to NAPRT are needed to induce its expression.

Among the potential EMT signaling pathways in which NAPRT participates, Wnt/β-catenin signaling was significantly increased in the EMT gastric cancer cell lines ($P = .0027$ by Kolmogorov-Smirnov test; Figure 6*C*) and TMA samples ($P < .001$ by Student t test; Figure 6*D*). Wnt signaling promotes tumor cell invasion and metastasis through the stabilization and nuclear translocation of β-catenin.[19] Accumulating evidence also indicates that β-catenin plays a central role in regulating EMT.[19,20] In agreement with these previous observations, we found that treatment with transforming growth factor-β, a well-known driver of gastric cancer invasion and metastasis,[21] induced EMT signaling and stabilized β-catenin in non-EMT gastric cancer cell lines, consistent with the involvement of this protein in gastric cancer EMT signaling (Supplementary Figure 8*A*). In addition, we found that the ectopic expression of *NAPRT* in EMT gastric cancer cell lines lowered the protein levels of β-catenin and those of Wnt/β-catenin downstream targets cyclin D1 and B1, c-MYC, AXIN2, and matrix metalloproteinase 7 compared with EMT gastric cancer cell lines that did not express *NAPRT* (Figure 6*E*). In contrast, small interfering RNA–mediated depletion of NAPRT in non-EMT gastric cancer cell lines increased the accumulation of β-catenin and its target proteins (Figure 6*F*).

The canonical function of NAPRT is to catalyze a reaction that converts nicotinic acid to nicotinic acid mononucleotide, a precursor of NAD. Intriguingly, supplementation of the EMT gastric cancer cell lines with NAD at a concentration that rescued the FK866 toxicity did not affect the levels of β-catenin and its targets (Supplementary Figure 8*B*), indicating that the effect of NAPRT on β-catenin signaling is independent of its function in NAD biosynthesis. After ectopic expression of *NAPRT* in EMT gastric cancer cell lines, we observed decreased levels of nuclear and cytoplasmic β-catenin (Figure 6*G*); nuclear localization of β-catenin is considered a hallmark of Wnt activation.[22] The decrease in β-catenin by ectopic expression of *NAPRT* was prevented by the addition of a proteasome inhibitor, bortezomib, indicating that NAPRT destabilizes β-catenin at the protein level (Figure 6*H*). In contrast, when NAPRT was depleted in non-EMT gastric cancer cell lines, the nuclear localization of β-catenin increased (Figure 6*I*). Collectively, these findings suggested that loss of *NAPRT* expression in EMT gastric cancer is not a passenger alteration but functions as a driver that activates Wnt/β-catenin signaling and, as a consequence, renders the cells dependent on NAMPT for the synthesis of NAD^+ for survival (Figure 6*J*).

Taken together, these results suggest that the downregulation of NAPRT in a broad array of EMT-subtype gastric tumors contributes to EMT activation through stabilization of β-catenin and activation of its downstream signaling and simultaneously makes them dependent on the function of NAMPT to maintain intracellular NAD levels, thereby providing a potential synthetic lethal target in the EMT-subtype gastric cancer and possibly other cancers.

Discussion

Current understanding of the biological function of NAPRT is mostly limited to the context of NAD biosynthesis. NAPRT and NAMPT, the 2 main NAD salvage enzymes, catalyze reactions required for synthesizing NAD^+ in parallel using nicotinic acid and nicotinamide, respectively. Because NAD is an essential metabolite for cell survival, the suppression of *NAPRT* expression makes cells dependent on NAMPT. This synthetic lethal relation between NAPRT depletion and NAMPT inhibition has been reported previously.[13] In this study, we further discovered that NAPRT expression is lost in a wide range of EMT-subtype gastric tumors, thus providing novel insight into a potential

Figure 6. Loss of NAPRT expression is causally linked to EMT through activation of Wnt/β-catenin signaling. (*A*) The effect of ectopic *NAPRT* expression on the accumulation of the indicated proteins in the indicated cells at 48 hours after transfection (*NAPRT* cDNA [+; 1 μg] or empty vector [–]). (*B*) The effect of siRNA-mediated depletion of *NAPRT* on the accumulation of the indicated proteins in the indicated cells at 72 hours after transfection. (*C*) Gene set enrichment analysis showed activation of Wnt/β-catenin pathway genes in the EMT gastric cancer cell lines ($P = .0027$). (*D*) Comparison of Wnt/β-catenin target gene expression scores in EMT and non-EMT tumor samples. *Boxplot* as in Figure 4*A*. (*E*) As in *A*. (*Right panel*) Individual protein levels were quantified. Error bars indicate ±SD (n = 3). *$P < .05$ by Student t test. (*F*) As in *B*. (*Right panels*) Individual protein levels were quantified. The siNC is the negative control siRNA, and si*NAPRT* 1 and 2 are 2 different siRNA oligos targeting *NAPRT*. Error bars indicate ±SD (n = 3). *$P < .05$ by Student t test. (*G*) As in *E*, except that cytoplasmic and nuclear fractions of cell lysates were used. β-Actin and lamin B1 were used as cytoplasmic and nuclear markers, respectively. (*H*) As in *A*, except that the cells were cotreated with bortezomib (50 nmol/L) or vehicle (dimethyl sulfoxide) for 24 hours after 12 hours of transfection. (*I*) As in *F*, except that cytoplasmic and nuclear fractions of MKN45 lysates were used. (*J*) A schematic model of synthetic lethality in EMT-activated cancers. In EMT-activated cells, NAPRT expression is suppressed, which stabilizes β-catenin, rendering them susceptible to the NAMPT inhibitor FK866. In non-EMT or normal cells, NAPRT is expressed at normal levels, making them resistant to FK866. Cyto, cytoplasmic; MMP7, matrix metalloproteinase 7; NAMN, Nicotinic acid mononucleotide; NMN, Nicotinamide mononucleotide; Nuc, nuclear.

therapeutic approach for this treatment-refractory cancer subtype (Figure 6J).

In addition to marked differences in the molecular and cellular phenotypes between EMT and non-EMT gastric cancer cell lines, a certain degree of heterogeneity is observed within these subtypes. One example is CD44 expression. Although *CD44* is under positive regulation by Snail and ZEB1,[23–25] it also is negatively regulated by wild-type p53.[26] In line with this, all 3 EMT gastric cancer cell lines expressing the highest levels of CD44 carried mutant p53 (Figure 1D), whereas SNU1750 and SNU484, which carried wild-type p53, did not express or expressed low levels of CD44 (Figure 2A). Another example is quantitative differences in rates of Matrigel invasion and sphere formation within subtypes. MKN1, which belongs to the EMT subtype, exhibited lower rates of Matrigel invasion and sphere formation than other EMT-subtype cells (Supplementary Figure 2A and 2B). Moreover, 2 non-EMT cell lines, AGS and SNU719, displayed higher rates of Matrigel invasion and sphere formation than their non-EMT counterparts (Supplementary Figure 2A and 2B). Our data suggest that these might, at least in part, be explained by differences in the expression levels of Snail and ZEB1, which are key drivers of invasion and sphere formation[7]: MKN1 markedly expressed low levels of Snail and ZEB1, whereas AGS and SNU719 expressed relatively high levels of Snail (Figure 2A). Collectively, some of the quantitative differences among the EMT-associated phenotypes are most likely attributable to co-segregating mutations or expression levels of key transcription factors, such as Snail and ZEB1.

EMT-subtype gastric cancer cell lines display the full EMT characteristics (ie, depletion of epithelial proteins and increase of mesenchymal proteins; Figure 3A). However, NAPRT depletion also is found in some gastric cancer cell lines and TMA samples that exhibit partial EMT characteristics but belong to the non-EMT subtype. For example, 4 of the 5 exceptional non-EMT cell lines displaying NAPRT deficiency and sensitivity to FK866 expressed high levels of Snail and epithelial proteins at the same time (Supplementary Figure 4A). In addition, non-EMT tumors in the TMA exhibited positive correlations in gene expression between *NAPRT* and *CDH1* (Supplementary Figures 6D). At the protein level, tissues with weak E-cadherin positivity tended to express significantly lower levels of NAPRT (Table 1). Likewise, 8 of 10 vimentin-positive tumors showed NAPRT negativity (n = 6) or weak positivity (n = 2). The paucity of vimentin positivity in TMA samples is likely due to the absence of sarcomatoid transformation, which forms spindle-like cells and is observed in lung, renal, and liver cancer but not in gastric cancer.[27] These data collectively suggest that downregulation of NAPRT is a continuous process that begins in a partial EMT stage (characterized by incomplete depletion of epithelial marker proteins and expression of the EMT transcription factor Snail) and is most readily observable in the full EMT stage. In addition, because NAPRT suppresses EMT through destabilization of β-catenin, we propose that *NAPRT* could play a part in tumor-suppressive function by inhibiting EMT activation in gastric cancer and potentially other cancers.

Because β-catenin stability is primarily regulated by the β-catenin destruction complex, consisting of Axin, APC, GSK3, and CKI,[28] NAPRT might exert a tumor-suppressive role by stabilizing the β-catenin destruction complex. Further studies are needed to test this hypothesis and elucidate the detailed molecular mechanisms.

Although several NAMPT inhibitors, including FK866, have completed phase I clinical trials for advanced forms of cutaneous T-cell lymphoma and melanoma and refractory B-cell chronic lymphocytic leukemia, these compounds have not progressed further, because they have poor clinical responses even at doses associated with toxicities, including thrombocytopenia and gastrointestinal symptoms.[12] In rodent safety studies, highly potent NAMPT inhibitors also displayed on-target retinal and cardiac toxicities, which were not reported in human clinical trials, suggesting they might occur at higher doses than those used in clinical trials.[12] Although cotreatment with nicotinic acid, in an attempt to increase the therapeutic index, rescued some of the toxicities in animals, it led to a loss of antitumor efficacy, most likely from complementation by exogenous NAD generated in normal tissues using supplemented nicotinic acid.[13] Thus, identifying patients whose tumors show stronger dependence on NAMPT relative to normal tissue might be critical to the success of treatments using NAMPT inhibitors. However, previous clinical trials apparently did not take this into account when selecting cancer types and patients.[17,29] Thrombocytopenia and lymphocytopenia were previously observed in treatment with FK866 at 60 and 40 mg/kg in mice, respectively,[30] doses that were 3- and 2-fold higher than the effective concentration observed in our tumor xenograft study. This indicates that, because gastric cancer of the EMT subtype displays the most prominent suppression of NAPRT, the safety margin of NAMPT inhibitors might be maximized in this context, allowing for effective treatment at lower doses to lessen the likelihood of documented toxicities.

In conclusion, our findings hold tremendous translational implications with respect to novel treatment options for EMT-subtype tumors that, in various contexts, are refractory to known treatments. Further studies might be needed to validate these findings in other cancer types.

Supplementary Material

References

1. Cancer Genome Atlas Research Network. Comprehensive molecular characterization of gastric adenocarcinoma. Nature 2014;513:202–209.

2. Cristescu R, Lee J, Nebozhyn M, et al. Molecular analysis of gastric cancer identifies subtypes associated

with distinct clinical outcomes. Nat Med 2015;21:
449–456.

3. Herbertz S, Sawyer JS, Stauber AJ, et al. Clinical development of galunisertib (LY2157299 monohydrate), a small molecule inhibitor of transforming growth factor-beta signaling pathway. Drug Des Devel Ther 2015; 9:4479–4499.

4. Kahn M. Can we safely target the WNT pathway? Nat Rev Drug Discov 2014;13:513–532.

5. Andersson ER, Lendahl U. Therapeutic modulation of Notch signalling—are we there yet? Nat Rev Drug Discov 2014;13:357–378.

6. Du B, Shim JS. Targeting epithelial-mesenchymal transition (EMT) to overcome drug resistance in cancer. Molecules 2016;21(7).

7. **Mani SA, Guo W, Liao MJ**, et al. The epithelial-mesenchymal transition generates cells with properties of stem cells. Cell 2008;133:704–715.

8. **Canto C, Menzies KJ**, Auwerx J. NAD(+) metabolism and the control of energy homeostasis: a balancing act between mitochondria and the nucleus. Cell Metab 2015; 22:31–53.

9. Hasmann M, Schemainda I. FK866, a highly specific noncompetitive inhibitor of nicotinamide phosphoribosyltransferase, represents a novel mechanism for induction of tumor cell apoptosis. Cancer Res 2003; 63:7436–7442.

10. Tan B, Young DA, Lu ZH, et al. Pharmacological inhibition of nicotinamide phosphoribosyltransferase (NAMPT), an enzyme essential for NAD+ biosynthesis, in human cancer cells: metabolic basis and potential clinical implications. J Biol Chem 2013;288:3500–3511.

11. **Choi YY, Lee JE**, Kim H, et al. Establishment and characterisation of patient-derived xenografts as paraclinical models for gastric cancer. Sci Rep 2016; 6:22172.

12. Sampath D, Zabka TS, Misner DL, et al. Inhibition of nicotinamide phosphoribosyltransferase (NAMPT) as a therapeutic strategy in cancer. Pharmacol Ther 2015; 151:16–31.

13. **O'Brien T, Oeh J, Xiao Y**, et al. Supplementation of nicotinic acid with NAMPT inhibitors results in loss of in vivo efficacy in NAPRT1-deficient tumor models. Neoplasia 2013;15:1314–1329.

14. Tateishi K, Wakimoto H, Iafrate AJ, et al. Extreme vulnerability of IDH1 mutant cancers to NAD+ depletion. Cancer Cell 2015;28:773–784.

15. Ooi CH, Ivanova T, Wu J, et al. Oncogenic pathway combinations predict clinical prognosis in gastric cancer. PLoS Genet 2009;5:e1000676.

16. Jones PA. Functions of DNA methylation: islands, start sites, gene bodies and beyond. Nat Rev Genet 2012; 13:484–492.

17. **Shames DS, Elkins K, Walter K**, et al. Loss of NAPRT1 expression by tumor-specific promoter methylation provides a novel predictive biomarker for NAMPT inhibitors. Clin Cancer Res 2013;19:6912–6923.

18. **Brabletz T, Kalluri R, Nieto MA**, et al. EMT in cancer. Nat Rev Cancer 2018;18:128–134.

19. Eger A, Stockinger A, Schaffhauser B, et al. Epithelial mesenchymal transition by c-Fos estrogen receptor activation involves nuclear translocation of beta-catenin and upregulation of beta-catenin/lymphoid enhancer binding factor-1 transcriptional activity. J Cell Biol 2000; 148:173–188.

20. **Liu W, Xing F**, Iiizumi-Gairani M, et al. N-myc downstream regulated gene 1 modulates Wnt-beta-catenin signalling and pleiotropically suppresses metastasis. EMBO Mol Med 2012;4:93–108.

21. Mishra L, Shetty K, Tang Y, et al. The role of TGF-beta and Wnt signaling in gastrointestinal stem cells and cancer. Oncogene 2005;24:5775–5789.

22. Henderson BR. Nuclear-cytoplasmic shuttling of APC regulates beta-catenin subcellular localization and turnover. Nat Cell Biol 2000;2:653–660.

23. **Nieto MA, Huang RY, Jackson RA**, et al. Emt: 2016. Cell 2016;166:21–45.

24. Huang L, Wu RL, Xu AM. Epithelial-mesenchymal transition in gastric cancer. Am J Transl Res 2015;7:2141–2158.

25. Ryu HS, Park DJ, Kim HH, et al. Combination of epithelial-mesenchymal transition and cancer stem cell-like phenotypes has independent prognostic value in gastric cancer. Hum Pathol 2012;43:520–528.

26. Godar S, Ince TA, Bell GW, et al. Growth-inhibitory and tumor-suppressive functions of p53 depend on its repression of CD44 expression. Cell 2008;134:62–73.

27. Otsuki S, Inokuchi M, Enjoji M, et al. Vimentin expression is associated with decreased survival in gastric cancer. Oncol Rep 2011;25:1235–1242.

28. Clevers H, Nusse R. Wnt/beta-catenin signaling and disease. Cell 2012;149:1192–1205.

29. **Goldinger SM, Gobbi Bischof S**, Fink-Puches R, et al. Efficacy and safety of APO866 in patients with refractory or relapsed cutaneous T-cell lymphoma: a phase 2 clinical trial. JAMA Dermatol 2016;152:837–839.

30. Olesen UH, Thougaard AV, Jensen PB, et al. A preclinical study on the rescue of normal tissue by nicotinic acid in high-dose treatment with APO866, a specific nicotinamide phosphoribosyltransferase inhibitor. Mol Cancer Ther 2010;9:1609–1617.

31. **Freese NH, Norris DC**, Loraine AE. Integrated genome browser: visual analytics platform for genomics. Bioinformatics 2016;32:2089–2095.

BASIC AND
TRANSLATIONAL AT

Supplementary Methods

Cell Line Authentication

All gastric cancer-cell lines, except for SK4 and the Yonsei Cancer Center (YCC)-series cell lines, were purchased from the Korea Cell Line Bank. SK4 cells were a kind gift from Dr. Julie Izzo (MD Anderson Cancer Center). YCC-series cell lines were obtained from the Song-Dang Institute for Cancer Research, Yonsei University College of Medicine. The cells were grown in RPMI-1640 medium supplemented with 10% fetal bovine serum (Gibco) and 1% penicillin–streptomycin (Invitrogen). The absence of mycoplasma contamination was confirmed in all cell lines by using a Mycoplasma detection kit (R&D Systems). To authenticate the 29 gastric cancer cell lines, we used the AmpFLSTR Identifiler PCR Amplification kit (Applied Biosystems) to detect 16 short tandem repeat (STR) loci. The resulting STR profiles were cross-compared and matched with deposited STR information. Cell line authentication results are provided in Supplementary Table 1.

Whole Exome Sequencing (WES)

Genomic DNA was extracted from the 29 gastric cancer cell lines by using a QIAamp DNA Mini Kit according to the manufacturer's instructions (QIAGEN). Whole-exome capture was performed using a SureSelect Human All Exon V4 51Mb Kit (Agilent Technologies). Captured DNA was sequenced using the HiSeq 2500 platform (Illumina) to generate at least 98.9 million paired-end sequencing reads of 100 bp per sample. The paired-end reads were aligned to the UCSC human reference genome assembly (GRCh37/hg19) with the Burrows-Wheeler Alignment (BWA) tool[1] using the default parameters. On average, 98.3% of the reads were successfully aligned to the human genome. After removal of duplicate reads with the Picard package (http://broadinstitute.github.io/picard/), Genome Analysis Tool Kit (GATK) version 3.4-46 was used for recalibration of read quality scores and local realignment to identify short insertions and deletions (indels) by using the HaplotypeCaller package and to filter variants on the basis of GATK Best Practices quality control filters[2]. Single nucleotide variants (SNVs) were identified using Mutect[3] (tumor-only option and otherwise default parameters). Variants supported by at least five high-quality reads (Phred-scaled quality score > 30) and detected with at least a 20% allele frequency were selected for further analysis. The detected SNVs and indels were annotated using the single nucleotide polymorphism (SNP) database (dbSNP, build 147)[4], 1000 Genomes Project (Phase 3)[5], Exome Sequencing Project (build 20141103)[6], Korean dbSNP (build 20140512)[7], and somatic mutations of TCGA gastric cancer (n = 395) (http://cancergenome.nih.gov/) using Variant Effect Predictor software (VEP, version 87)[8]. Regions of known germline chromosomal segmental duplication[9] and tandem repeats[10] were annotated using ANNOVAR[11]. Variants were filtered to exclude germline polymorphisms, chromosomal segmental duplications and tandem repeats. Variants were subsequently filtered to include known somatic mutations observed in at least 12 samples of the TCGA gastric cancer dataset, and nonsynonymous mutations observed in genes belonging to the Cancer Gene Census[12] reported by at least ten samples in the COSMIC database (version 87)[13]. WES data were deposited in NCBI SRA (#SRP078289). For analyzing cell line ontology, unsupervised hierarchical clustering was conducted on the basis of pairwise distance (1 - concordance rate of SNPs) with complete linkage.

RNA Sequencing

Total RNA was extracted from the 29 gastric cancer cell lines with an RNeasy Plus Mini Kit according to the manufacturer's instructions (QIAGEN). The mRNA-focused libraries were generated with a TruSeq RNA Sample Prep kit v2 (Illumina) and sequenced with the HiSeq 2500 platform to obtain at least 40 million paired-end reads of 100 bp per sample. The TopHat-Cufflinks[14] pipeline was used to align the reads to the reference genome and to calculate normalized gene expression values in FPKM (fragments per kilobase of exon per million fragments mapped). RNA-seq data were deposited in NCBI SRA (#SRP078289).

Mutation Analyses

A total of 11,469 SNVs in the 29-gastric cancer cell lines were detected among exons and exon-intron boundaries after rigorous filtering of putative germline variants reported in various public repositories, potential false positives detected in regions of germline chromosomal segmental duplication and tandem repeats (Supplementary Data 1).

Normalization and Pre-processing of Public Gene Expression Data

We collected gene expression profiles from 31 cohorts (sample size > 100) representing 17 major tumor types (Supplementary Data 3). We normalized the E-MTAB-923 dataset in CEL format with the robust multichip average method using the affy R package. Otherwise, the microarray datasets were downloaded as normalized expression values on a $\log_2$ scale. Similarly, upper quartile normalized FPKM values for RNA-seq datasets were transformed by $\log_2$ (FPKM + 1). Duplicate entries per sample were collapsed by calculating median expression values for the duplicates. Additionally, basal gene expression microarray datasets were downloaded, quantile-normalized, and $\log_2$-transformed for 178 of the 942 tissue microarray (TMA) samples measured by the Illumina HumanHT-12 V3.0 platform[15] (GEO accession GSE 84437).

Meta-analysis of the Tumor Datasets

A total of 14 datasets for five tumor types (breast cancer, colorectal cancer, lung adenocarcinoma, pancreatic ductal adenocarcinoma and stomach adenocarcinoma) were eligible for meta-analysis because they included at least two independent datasets in which a significant fraction of their respective samples (> 3%) displayed significantly high EMT signature scores in the q-q plot. We conducted a random-effects meta-analysis to test the statistical significance of

differences in *NAPRT* expression levels between samples with high EMT signature scores and the rest of the samples across multiple independent studies for individual tumor types. A random-effects model assumes that the effects estimated in the heterogeneous studies are not identical; thus, an unbiased standardized mean difference[9] was used to represent an overall effect-size, taking into account between-study variance and within-study variance in estimating combined probabilities. We used the MetaDE R package[10] for the meta-analysis with default parameters (number of permutations = 1,000, unpaired design).

Immunohistochemistry for Primary and Metastatic Tumor Samples

Tumors were fixed in 10% formalin for 12 hours. After ethanol dehydration, tissues were cleared with xylene and embedded in paraffin. Four-micrometer thick sections were attached to slides, boiled for antigen retrieval in 10 mM citrate buffer (pH 6) at 100°C for 10 min after deparaffination and rehydration and incubated for 10 minutes with 3% hydrogen peroxide in methanol to block endogenous peroxidase activity. After being washed in TBS, the slides were incubated for 30 minutes with blocking solution (5% BSA) and incubated overnight at 4°C with anti-NAPRT antibody (Novus Biologicals, #NBP1-87243) or anti-E-cadherin antibody (Leica Biosystems, E-CAD-L-CE) diluted 1:100 in blocking solution. This was followed by incubation for 20 minutes with anti-rabbit IgG antibody (DAKO, #k4003). The slides were subsequently washed with PBS, covered with 0.3 μg/μl 3,3'-diaminobenzidene (DAB) to visualize the bound antibodies, and counterstained with hematoxylin for 1 minute. After being cleared with a graded ethanol series and xylene, the slides were permanently mounted. Observation and photography were conducted using a DM2000 microscope equipped with a DFC320 digital imaging system (Leica). The expression level of NAPRT was semi-quantitatively evaluated by assessing the intensity of the cytoplasmic staining in the tumor cells by eye, using scoring of negative (0), weak positivity (1+), moderate positivity (2+) or strong positivity (3+). E-cadherin staining was evaluated by assessing diffuse membranous staining in tumor cells by eye, using scoring of negative (0), weak positivity (1+), or strong positivity (2+). Focal weak membranous, cytoplasmic, nuclear, or Golgi staining was considered negative.

Methylation-specific PCR

The DNA methylation status of the CpG islands in the *NAPRT* promoter region was determined with PCR analysis of sodium bisulfite-treated genomic DNA (gDNA). Bisulfite-modified gDNA was prepared using an EZ DNA Methylation-Lighting kit (Zymo Research, USA) according to the manufacturer's instructions. Methylated and unmethylated *NAPRT* DNA-specific primers were designed using Meth-Primer software[16]. The methylated primers used were 5'-TTGGTAGAG GTTAGTGAGTAGCGGTCGC-3' and 5'-GAACGTCGA AAACAAAATAACGACGAA-3' and the unmethylated primers were 5'-TTTGGTAGAGGTTAGTGAGTAGTGGTTGTG-3' and 5'-CCAAACATCAAAAACAAAATAACAACAAA-3'. The PCR mix contained 2.5 μl of 10X Taq buffer, 2.5 unit nTaq polymerase (Enzynomics), 2 μl of dNTP mix (2.5 mM each), 2 μl of each primer (10 pmole/μl), and bisulfite-treated gDNA (50 ng). The PCR conditions used were 10 min at 95°C, 38 cycles of 30 sec at 95°C, 30 sec at either 60°C (for unmethylated primers) or 62°C (for methylated primers), 30 sec at 72°C, followed by final extension at 72°C for 5 min. The PCR products (4 μl) were resolved on a 2% agarose gel using TBE buffer.

Analysis of CpG Island Methylation in the NAPRT Promoter

For the analysis of CpG island methylation in the *NAPRT* promoter region in the tumor dataset, we downloaded DNA methylation data of the TCGA stomach adenocarcinoma (STAD) project from the NCI's Genomic Data Commons (GDC) (https://gdc.cancer.gov/). The data were generated with Illumina Human Methylation 450 (n = 397) and Illumina Human Methylation 27 (n = 73). A total of 338 samples with both methylation and transcriptome (RNA-seq) information were eligible for the analysis. The DNA methylation score for each CpG site of the *NAPRT* promoter was estimated as a beta (β) value (β = methylated / (methylated + unmethylated)). The β value was subsequently mean centered across samples for each CpG site. Pearson's correlation test was conducted to assess the statistical significance of the correlation between *NAPRT* expression levels and methylation status of each site. The cumulative methylation enrichment score of *NAPRT* for each sample was calculated by cumulatively adding the mean of mean-centered ß values across the CpG sites of the samples sorted in ascending order of *NAPRT* expression values.

Gene Set Enrichment Analysis

We performed gene set enrichment analysis (GSEA)[17] between EMT and non-EMT gastric cancer cell lines by using $\log_2$ (FPKM +1) values of RNA-seq data using the GSEA software against the C2 curated gene sets of canonical pathways in the Molecular Signature Database (MsigDB, curated version 5.2) (http://software.broadinstitute.org/gsea/msigdb/index. jsp). The statistical significance of normalized enrichment scores (NES) to each gene set was assessed using a phenotype-based permutations test (n = 1,000). Tumor-specific Wnt signaling activity scores were calculated using GenePattern's Single-sample GSEA (ssGSEA) method[18] for genes belonging to the KEGG_WNT_SIGNALING_PATHWAY in MsigDB.

Copy Number Analysis

Bam files from whole-exome sequencing (WES) of 26/29 gastric cancer cell lines were used to generate gene-based read-count matrices using Bedtools[19], according to the UCSC hg19 refgene table[20]. Next, the numeral 1 was added to the read-counts to prevent negative infinite values in $\log_2$ transformation. Genes which had median read-counts below 20 were filtered out. The read-counts were

normalized to the trimmed mean of the M-values normalization method using edgeR[21] and divided by the median read-counts corresponding to each gene to calculate $\log_2$-ratio values. A circular binary segmentation algorithm was implemented with the $\log_2$-ratio values using the DNAcopy R package (Seshan & Olshen, 2016 DNAcopy: DNA copy number data analysis; R package version 1.46.0.). Genomic Identification of Significant Targets in Cancer (GISTIC) 2.0[22], with default parameters, was applied to the segmented data to identify regions that were frequently altered in DNA copy number.

Immunoblot Analysis

The cells were harvested, washed with PBS, and lyzed on ice with RIPA buffer containing protease inhibitors and Phosphatase Inhibitor Cocktail (GeneDepot). After incubation for 20 minutes, the cell lysates were centrifuged at 4 °C for 10 min at full speed. Resected patient tumor samples or tumor xenograft specimens were homogenized with lysis buffer at 4 °C. Cellular debris was subsequently removed by centrifugation in a microfuge at full speed for 20 min at 4 °C. Protein concentrations were measured by using the Bradford method. Equal amounts of total protein were subjected to SDS gel electrophoresis and transferred to PVDF membranes. The membranes were blocked for one hour at room temperature and incubated overnight at 4 °C with primary antibody in buffer containing 0.1% Tween-20. Subsequently, the membranes were washed three times with Tween-TBS buffer and incubated with secondary antibody diluted in blocking buffer containing 0.1% Tween-20 for two hours at room temperature. The membranes were subsequently washed three times with Tween-TBS for 10 minutes each. Rabbit polyclonal anti-NAPRT antibody was obtained from Sigma-Aldrich (#HPA024017) and used at a 1:1,000 dilution; rabbit polyclonal anti-GRHL2 (#PA5-28973) and anti-Claudin-7 antibody (#34-9100) were obtained from thermos-scientific and used at a 1:2000 dilution; mouse monoclonal anti-CD44 antibody (#5640), rabbit monoclonal anti-phospho-SMAD 2/3 antibody (#8828), anti-SMAD 2/3 antibody (#8685), anti-β-Catenin antibody (#8480), anti-Lamin B1 antibody (#13435), anti-Axin 2 antibody (#2151), anti-Cyclin D1 antibody (#2922), and anti-Snail antibody (#3879) were obtained from Cell Signaling and used at a 1:1,000 dilution; rabbit polyclonal anti-Fibronectin was obtained from Abcam (#ab2413) and used at a 1:1,000 dilution; monoclonal anti-Vimentin antibodies were obtained either from Novus (#NB100-74564) or from Cell Signaling (#5741) and used at a 1:2,000 or 1:1,000 dilution, respectively; mouse monoclonal anti-activated-β-Catenin antibody (#05-665) was obtained from Millipore and used at a 1:1,000 dilution; and rabbit polyclonal anti-E-cadherin antibody (#sc-7870), anti-EGFR antibody (#sc-03), anti-Cyclin B1 antibody (#sc-594), anti-c-myc antibody (#sc-789), anti-EpCAM antibody (#sc-25308), mouse monoclonal anti-beta-Actin antibody (#sc-47778), anti-Ubiquitin antibody (#sc-8017) and anti-MMP7 antibody (#sc-80205) were obtained from Santa Cruz Biotechnology and used at 1:1,000 to 1:5,000 dilutions. The relative abundance of individual proteins was measured by quantifying the intensities of individual protein bands on the immunoblots (relative to beta-actin) using ImageJ software.

cDNA Transfection

The pCMV6-GFP-NAPRT cDNA was purchased from Origene (#RG204356). Twenty-four hours before transfection, MKN1, SNU1750, SNU484 and SNU668 cells were plated at 300,000 cells per 35-mm dish and incubated at 37 °C. Transfection was performed by incubating the cells for 48 hours with NAPRT cDNA (with GFP tag) or empty vector using Lipofectamine 2000 (Invitrogen, Carlsbad, CA), according to the manufacturer's instructions. For investigating effects of NAPRT overexpression on FK866-dependent toxicity, cells were transfected with an empty vector (vec) or NAPRT cDNA. After 36 hours of transfection, the cells were exposed to FK866 for 72 hours. 100 μM nicotinic acid was added to the growth medium containing FK866 or vehicle.

Invasion Assay

Transwell chambers with an 8-μm pore size (Millipore) were coated with 300 μg/ml Matrigel. 1 x 10^5 cells in serum-free medium were plated into the upper chamber, and the bottom wells were filled with complete medium containing 10% FBS (Gibco). The cells were allowed to invade across the Matrigel-coated membrane for 48 hours at 37 °C in 5% CO_2. Subsequently, the cells were removed from the upper surface of the filter by scraping with a cotton swab. The invaded cells that adhered to the bottom of the membrane were fixed with methanol and stained with a 0.2% crystal violet solution. The average number of cells that penetrated the membrane was calculated from three randomly selected high-power fields (20X) and from three independent experiments.

Sphere Formation Assay

At 80% confluence, the cells were detached with trypsin–EDTA and re-plated at a density of 5×10^3 cells/well to ultra-low attachment six-well plates (Corning) containing serum-free DMEM-F12 medium supplemented with 20 ng/ml of epidermal growth factor (Invitrogen), 20 ng/ml of basic fibroblast growth factor (Invitrogen), and 2% of B27 supplement (Invitrogen). After one (SNU668) to two weeks (all other cell lines) of incubation, spheres greater than 50μm in diameter were counted under a phase-contrast microscope at 10X magnification[23]. The average number of spheres per 5,000 seeded cells was calculated from three independent experiments.

NAD/NADH Assay

To quantify NAD(H) in cell lines, the Ultra-Glo™ Recombinant Luciferase assay kit (Promega, #G9071) was used according to the manufacturer's instructions. Briefly, the cyclic enzyme included in the kit converts NAD^+ to NADH, which subsequently activates a reductase that

converts pro-luciferin to luciferin. The samples were subsequently detected with Ultra-Glo™ r-Luciferase. To this end, the cells were seeded into a 96-well culture plate at a density of 5×10^3 cells per well and incubated for 24 hours, then treated with FK866 for 40 hours. Subsequently, 50 μl of NAD/NADH-Glo™ Detection Reagent and an equal volume of sample were incubated at room temperature for 30 min. To quantify NAD(H) in tumor xenografts, a NAD/NADH colorimetric quantification kit (BioVision, #K337-100) was used according to the manufacturer's instructions. Briefly, 20 mg of the tissue sample was washed with ice-cold PBS and extracted with 400 μl of NAD/NADH extraction buffer. Total NAD signals of cells and tissues were measured at 450 nM (SpectraMax paradigm microplate reader) and normalized to the total protein concentrations which were determined using the Bradford assay.

Pharmacological Characterization

FDA-approved small molecule pharmacological compounds (#L1300) and investigational anti-cancer compounds (#L2000) were purchased from Selleckchem and supplied as 10 mM solutions in DMSO. A list of the tested compounds is provided in Supplementary Data 2. For the cell-based drug assay, sub-cultured cells were seeded onto 96-well white optical plates (Corning) at 5×10^3 cells per well. Twenty-four hours after seeding, either 2.5 μM (primary screen) or half-log 12-serial dilutions (secondary screen) of the pharmacological compound prepared in DMSO were robotically added to cells by using a BioMek FXp liquid handler (Beckman), thus yielding final drug concentrations ranging from 50 μM to 0.5 nM and a DMSO control (0.5%). The cells were further incubated at 37°C in a 5% CO_2 incubator for 72 hours before measuring cell viability using the CellTiter-Glo assay kit (Promega). Luminescence was measured after 15 minutes of incubation at room temperature using a SpectraMax Paradigm microplate reader equipped with a plate stacker. Viabilities normalized to DMSO controls[24] were used to generate a cell line-specific, 12-point dose-response curve for each pharmacological compound, and this was followed by calculation of area under the curve (AUC) using the trapezoidal method[25], in which a low AUC indicated high cell line sensitivity to the drug. The results from duplicate experiments were averaged to generate cell line-specific AUC values for each compound (Supplementary Data 2). In addition, the effects of NAPRT depletion on responses to FK866 treatment in SK4 and MKN45 cells were assessed by reverse transfection with si*NAPRT* (Ambion) or control siRNA (*TMEM114*, Dharmacon) by mixing 30 μl of 333 nM siRNA solution with 10 μl of 4% RNAiMax (Invitrogen) solution and incubating for 15 minutes. Subsequently, 5,000 cells in 100 μl growth medium were added to the siRNA-lipid mix. After 24 hours, the medium was replaced with fresh growth medium containing FK866, and the cells were further incubated for an additional 72 hours before measurement of cell viability.

Subcellular Fractionation

Subcellular fractionation was performed using the ProteoExtract® subcellular Proteome Extraction Kit according to the manufacturer's instructions (#539790, EMD Bioscience). Protein concentrations of the nuclear and cytosolic lysates were normalized following quantitation using the Bradford protein assay prior to SDS-PAGE and immunoblot analysis.

Xenograft Studies

Tumor xenografts derived from cell lines were established by subcutaneous injection of five million cells of the MKN45 cell line into the right flanks of female nude mice at 6 weeks of age. Once the tumor volume reached 200 mm^3, mice were randomly divided into three groups and administered twice daily intraperitoneal doses of FK866 (20 mg/kg, n = 6 or 25 mg/kg, n = 6) or vehicle (n = 5) for 24 days.

Immunohistochemistry for Xenograft Tumor Samples

The sections were deparaffinized in EZ Prep solution (Ventana) and the CC1 standard solution (Ventana) was used for antigen retrieval. First, the sections were blocked in inhibitor D (3% H_2O_2) for 4 min at 37 °C. The sections were incubated with primary antibody for 40 min followed by a universal secondary antibody for 20 minutes at 37°C. Streptavidin-horseradish peroxidase D was applied for 16 min, and the substrate 3,3′-diaminobenzidine tetrahydrochloride and H_2O_2 were added for 8 minutes, and this was followed by counterstaining with hematoxylin and a bluing reagent at 37°C.

Epstein-Barr Virus (EBV) Analysis

To detect EBV sequences in DNA and RNA for the 29 gastric cancer cell lines, reads with near perfect matches to the human genome were subsequently subtracted using BWA, allowing for a 20% and 30% mismatch, respectively. Next, unmapped reads were aligned to the UCSC EBV reference genome using BWA, allowing for a 2% mismatch. EBV-positive gastric cancer cell lines were determined based on number of mapped read counts for exome-seq > 300 and for RNA-seq > 3 (Supplementary Table 3).

Microsatellite Instability Analysis

Genomic DNA for each cell line was tested for five short tandem repeat (STR) markers with quasi-monomorphic mononucleotide repeats (BAT-25, BAT-26, NR-21, NR-22, and NR-24) using capillary electrophoresis with a 3730 DNA Analyzer (ABI capillary electrophoresis system)[26]. The results were subsequently analyzed using GeneMarker V2.2.0 software, as previously described[27]. The cell lines were considered as a microsatellite instability (MSI) subtype if they had three or more unstable microsatellites (Supplementary Table 2); otherwise, the cells were considered as a microsatellite stable (MSS) subtype.

References

1. **Li H**, Durbin R. Fast and accurate short read alignment with Burrows-Wheeler transform. Bioinformatics 2009; 25:1754–1760.
2. **McKenna A**, Hanna M, Banks E, et al. The Genome Analysis Toolkit: a MapReduce framework for analyzing next-generation DNA sequencing data. Genome Res 2010;20:1297–1303.
3. **Lawrence MS, Stojanov P, Polak P**, et al. Mutational heterogeneity in cancer and the search for new cancer-associated genes. Nature 2013;499:214–218.
4. **Sherry ST**, Ward MH, Kholodov M, et al. dbSNP: the NCBI database of genetic variation. Nucleic Acids Res 2001;29:308–311.
5. **Birney E, Soranzo N**. Human genomics: The end of the start for population sequencing. Nature 2015;526:52–53.
6. **Fu W**, O'Connor TD, Jun G, et al. Analysis of 6,515 exomes reveals the recent origin of most human protein-coding variants. Nature 2013;493:216–220.
7. **Kim JI**, Ju YS, Park H, et al. A highly annotated whole-genome sequence of a Korean individual. Nature 2009; 460:1011–1015.
8. **McLaren W**, Pritchard B, Rios D, et al. Deriving the consequences of genomic variants with the Ensembl API and SNP Effect Predictor. Bioinformatics 2010;26:2069–2070.
9. **She X**, Jiang Z, Clark RA, et al. Shotgun sequence assembly and recent segmental duplications within the human genome. Nature 2004;431:927–930.
10. **Gelfand Y**, Rodriguez A, Benson G. TRDB–the Tandem Repeats Database. Nucleic Acids Res 2007;35:D80–D87.
11. **Wang K**, Li M, Hakonarson H. ANNOVAR: functional annotation of genetic variants from high-throughput sequencing data. Nucleic Acids Res 2010;38:e164.
12. **Futreal PA**, Coin L, Marshall M, et al. A census of human cancer genes. Nat Rev Cancer 2004;4:177–183.
13. **Forbes SA**, Beare D, Boutselakis H, et al. COSMIC: somatic cancer genetics at high-resolution. Nucleic Acids Res 2017;45:D777–D783.
14. **Trapnell C**, Roberts A, Goff L, et al. Differential gene and transcript expression analysis of RNA-seq experiments with TopHat and Cufflinks. Nat Protoc 2012;7:562–578.
15. **Cheong JH**, Yang HK, Kim H, et al. Predictive test for chemotherapy response in resectable gastric cancer: a multi-cohort, retrospective analysis. Lancet Oncol 2018.
16. **Lal G**, Zhang N, van der Touw W, et al. Epigenetic regulation of Foxp3 expression in regulatory T cells by DNA methylation. J Immunol 2009;182:259–273.
17. **Subramanian A**, Tamayo P, Mootha VK, et al. Gene set enrichment analysis: a knowledge-based approach for interpreting genome-wide expression profiles. Proc Natl Acad Sci U S A 2005;102:15545–15550.
18. **Reich M, Liefeld T, Gould J**, et al. GenePattern 2.0. Nat Genet 2006;38:500–501.
19. **Quinlan AR**, Hall IM. BEDTools: a flexible suite of utilities for comparing genomic features. Bioinformatics 2010; 26:841–842.
20. **Karolchik D, Hinrichs AS**, Furey TS, et al. The UCSC Table Browser data retrieval tool. Nucleic Acids Res 2004;32:D493–D496.
21. **Robinson MD, McCarthy DJ**, Smyth GK. edgeR: a Bioconductor package for differential expression analysis of digital gene expression data. Bioinformatics 2010; 26:139–140.
22. **Mermel CH**, Schumacher SE, Hill B, et al. GISTIC2. 0 facilitates sensitive and confident localization of the targets of focal somatic copy-number alteration in human cancers. Genome Biol 2011;12:R41.
23. **Alajati A**, Guccini I, Pinton S, et al. Interaction of CDCP1 with HER2 enhances HER2-driven tumorigenesis and promotes trastuzumab resistance in breast cancer. Cell Rep 2015;11:564–576.
24. **Singh NK**, Seo BY, Vidyasagar M, et al. siMacro: A Fast and Easy Data Processing Tool for Cell-Based Genomewide siRNA Screens. Genomics Inform 2013; 11:55–57.
25. **Huang S**, Pang L. Comparing statistical methods for quantifying drug sensitivity based on in vitro dose-response assays. Assay Drug Dev Technol 2012;10: 88–96.
26. **Suraweera N**, Duval A, Reperant M, et al. Evaluation of tumor microsatellite instability using five quasimonomorphic mononucleotide repeats and pentaplex PCR. Gastroenterology 2002;123:1804–1811.
27. **Murata H**, Khattar NH, Kang Y, et al. Genetic and epigenetic modification of mismatch repair genes hMSH2 and hMLH1 in sporadic breast cancer with microsatellite instability. Oncogene 2002;21:5696–5703.

Author names in bold designate shared co-first authorship.
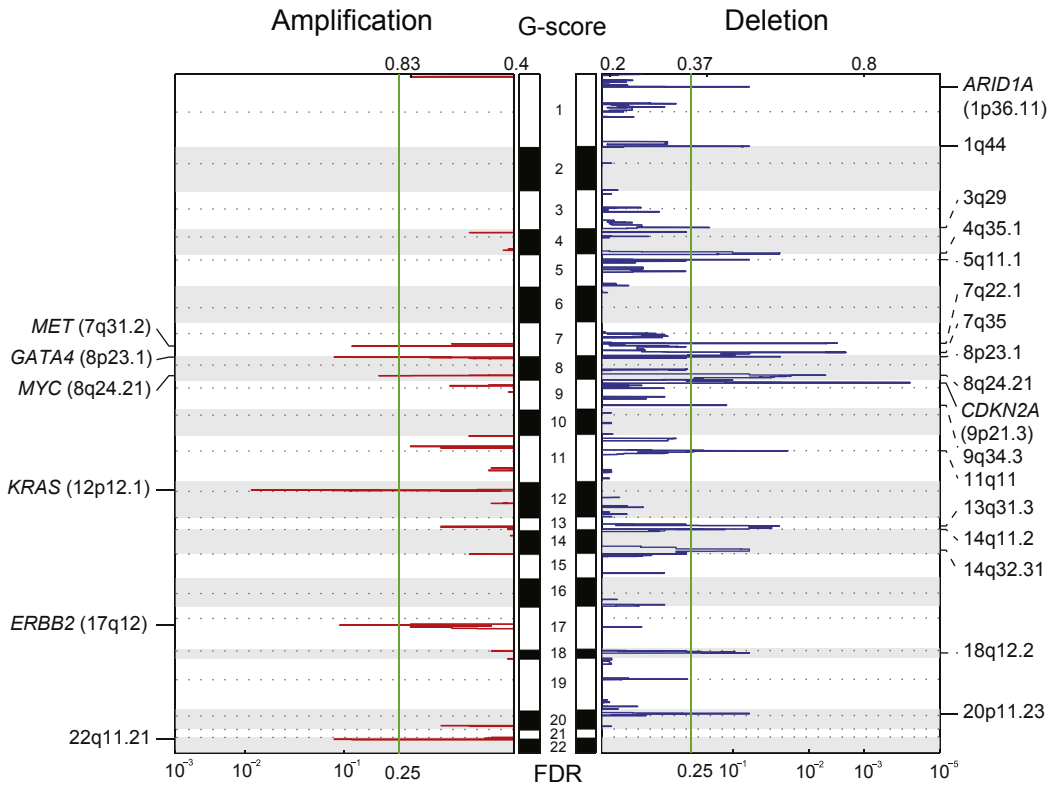
Supplementary Figure 1. Copy number alterations in gastric cancer cell lines mirror those found in primary tumors. The top x-axis indicates G-scores from GISTIC analysis, and the bottom x-axis indicates false discovery rate (FDR) scores. Chromosomal locations of peaks of recurring high-level amplifications (red) and deletions (blue) below FDR 0.25 are indicated, and candidate genes therein are shown. See Supplementary Data 1 for raw data.
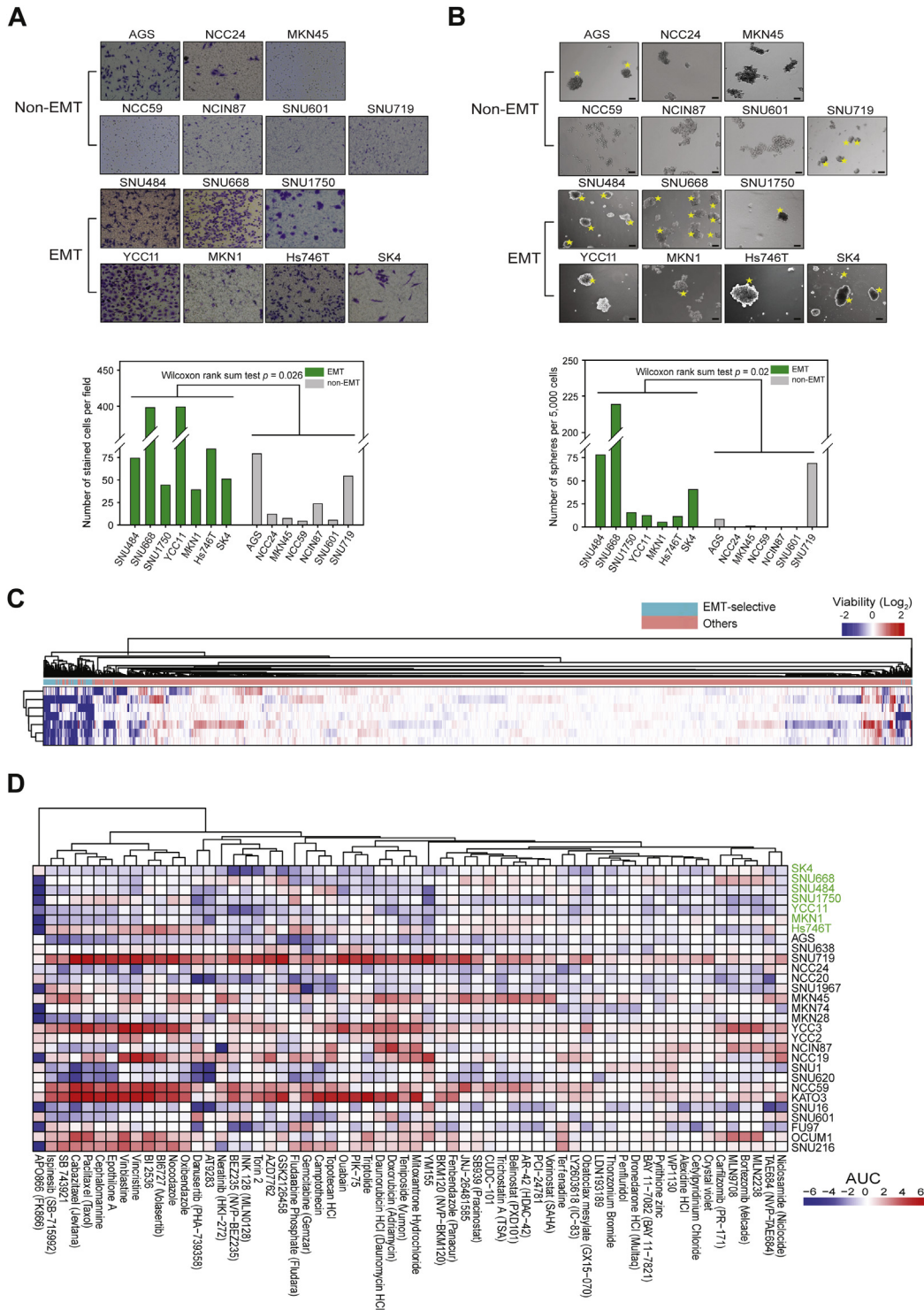
Supplementary Figure 2. Toxicity profiles for EMT-selective pharmacological compounds in the gastric cancer cell lines. (*A*) Matrigel Transwell invasion assay. Representative bright-field microscopic images for cells that invaded through Matrigel-coated transwell-membranes are shown in the upper panel and are quantified in the lower panel. Statistical differences between the EMT and non-EMT groups were determined by Wilcoxon rank sum test. (*B*) Tumor sphere-forming capabilities of gastric cancer cell lines. A tumor sphere was defined as a non-adherent colony of cells derived from a single cancer stem-like cell that was greater than 50 μm in diameter, as shown in the upper panel (indicated by yellow stars) and quantified in the lower panel. Scale bars represent 100 mm. Statistical differences between the EMT and non-EMT groups were determined by Wilcoxon rank sum test. (*C*) Unsupervised hierarchical clustering with complete linkage was used for clustering cell lines on the basis of log$_2$ viability scores for responses to a single concentration (2.5 μM) of each compound. See Supplementary Data 2 for raw data. Sixty-three compounds that showed toxicity (<50% viability) in four or more EMT gastric cancer cell lines (EMT-selective) are indicated in the bar below in cyan; others (n = 1,282) are shown in pink. (*D*) Unsupervised hierarchical clustering with complete linkage was used to cluster the 63 EMT-selective compounds on the basis of average area under the viability curve (AUC) values estimated from duplicate experiments and a 12-point dose-response analysis of cell viability for each of the 29 gastric cancer cell lines. See Supplementary Data 2 for the average AUC values, which were median centered for each compound. EMT gastric cancer cell lines are shown in green, and the other cell lines are shown in black.
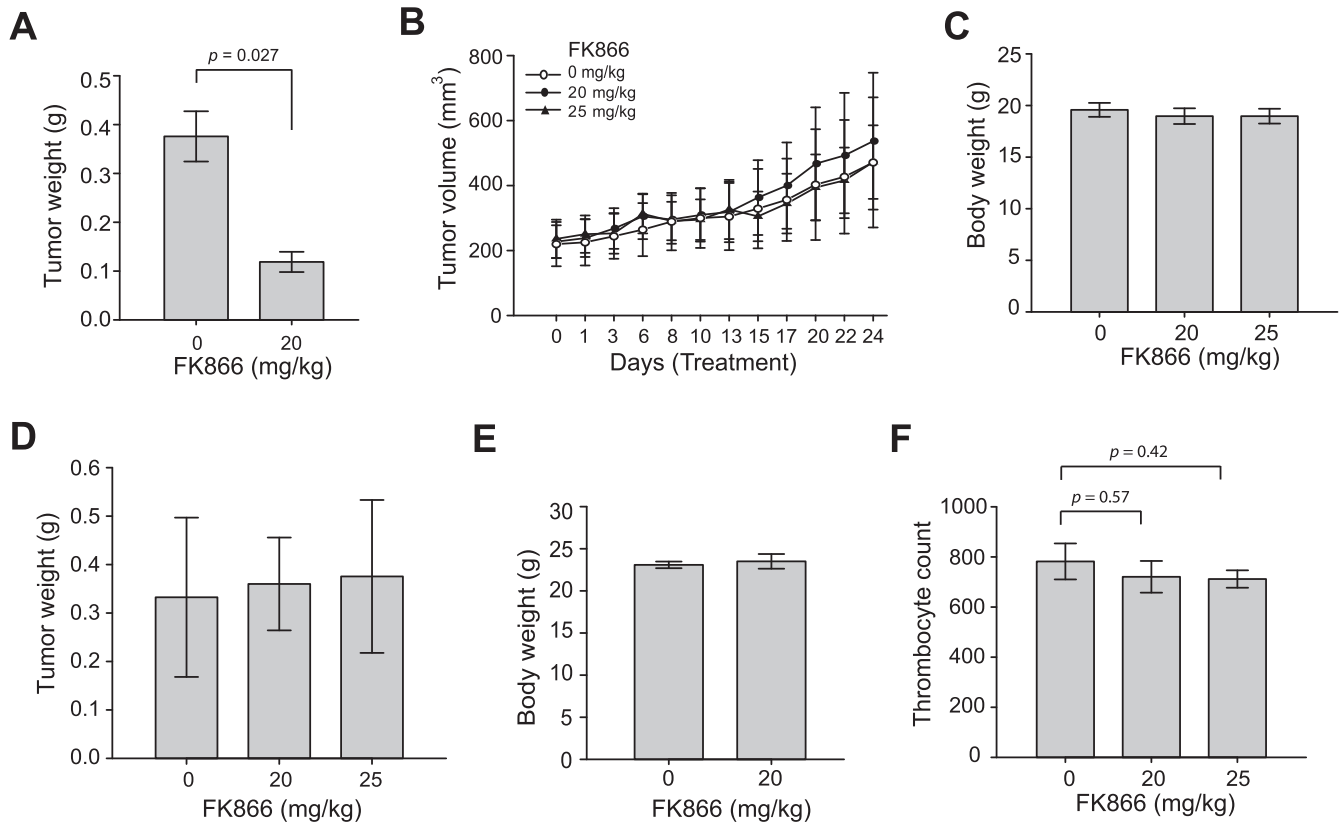
Supplementary Figure 3. Toxicity profile of FK866 in a non-EMT xenograft tumor model. (*A*) BALB/c-nude mice transplanted with GA077 were treated by intraperitoneal injection of FK866 (20 mg/kg, n = 5) or vehicle (n = 6) twice daily for 24 days. Tumor weights after 24 days of treatment. Error bars indicate ± SEM (n = 6). Student's t-test *p*-value is shown. (*B*) – (*D*) BALB/c-nude mice transplanted with non-EMT MKN45 cells were treated with intraperitoneal injections of FK866 (20 mg/kg or 25 mg/kg) or vehicle twice daily for 24 days. Tumor volume growth (*B*), body weight (*C*), and tumor weight (*D*) are shown. (*E*) Body weights after 24 days of treatment. Error bars indicate ± SEM (n = 6). (*F*) Thrombocyte count after 24 days of FK866 (20 or 25 mg/kg) or vehicle treatment. Error bars indicate ± SEM (n = 5 for vehicle and n = 6 for treated group).
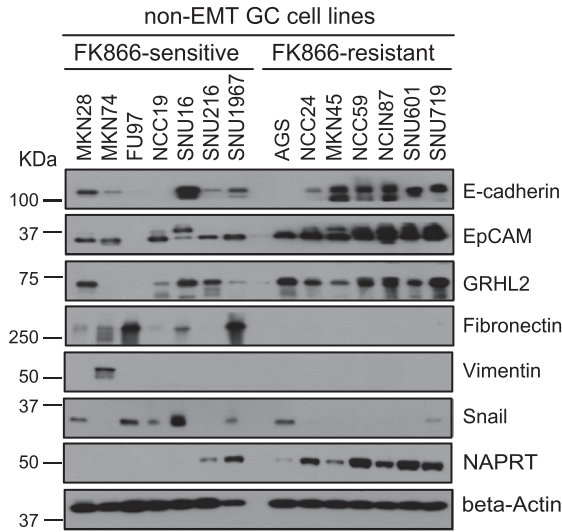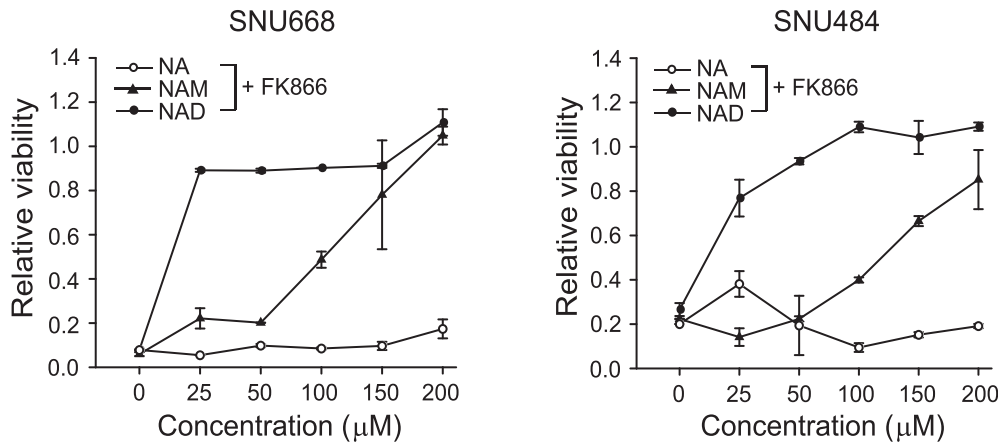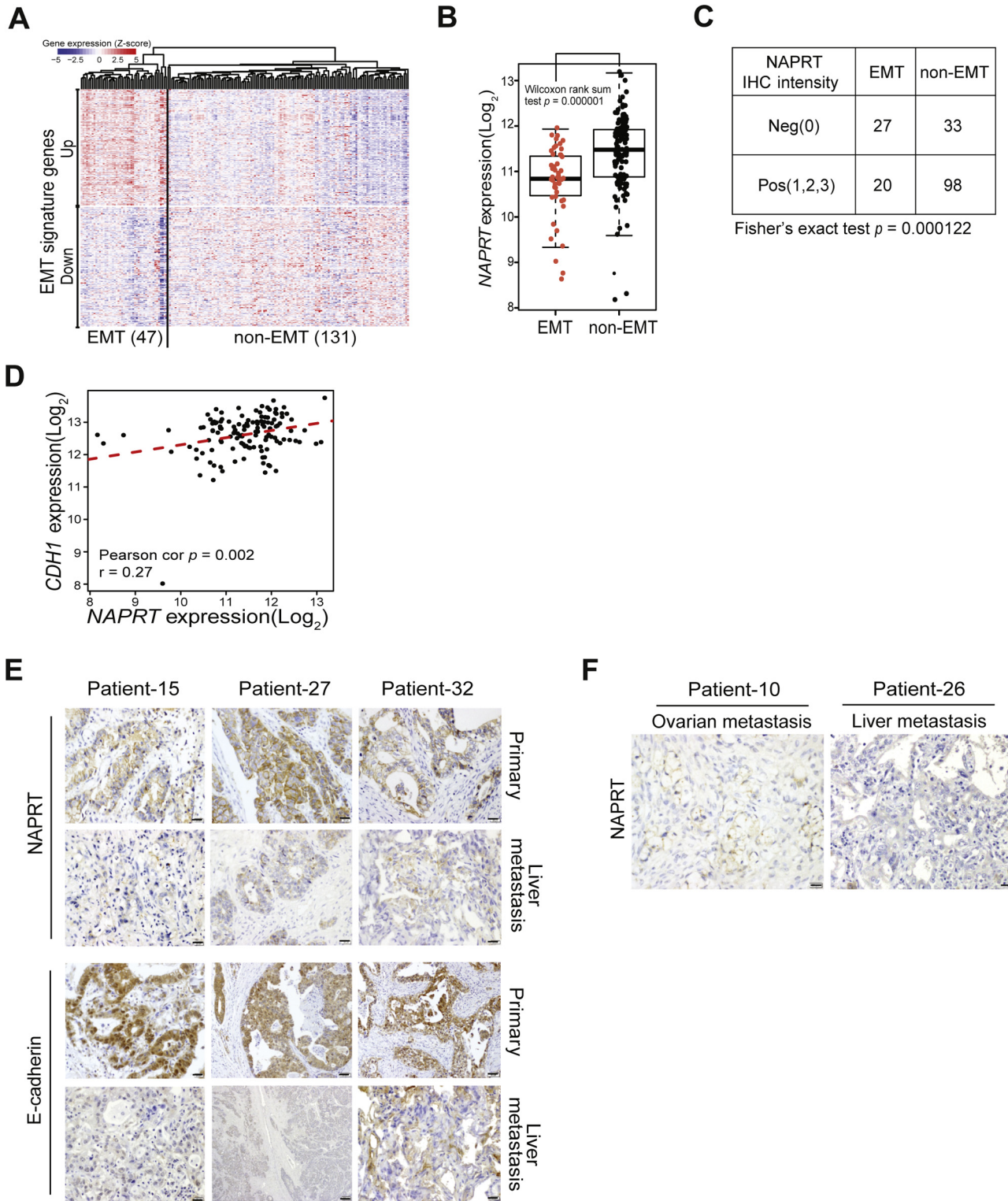
Supplementary Figure 4. Suppression of NAPRT expression generates synthetic lethality to NAMPT inhibition. (*A*) Molecular characterization of the seven FK866-sensitive non-EMT gastric cancer cell lines. Steady-state accumulation of the indicated proteins was assessed by immunoblotting of whole cell lysates from the indicated gastric cancer cell lines. beta-actin was utilized as a loading control. (*B*) EMT-subtype gastric cancer cell lines (SNU668 and SNU484) were treated with FK866 (25 nM) in addition to nicotinic acid (NA), nicotinamide (NAM), or NAD at the indicated concentrations and incubated for 72 hours. Cell viability was measured using the CellTiter-Glo assay (Promega). Error bars indicate ± SD (n = 3).
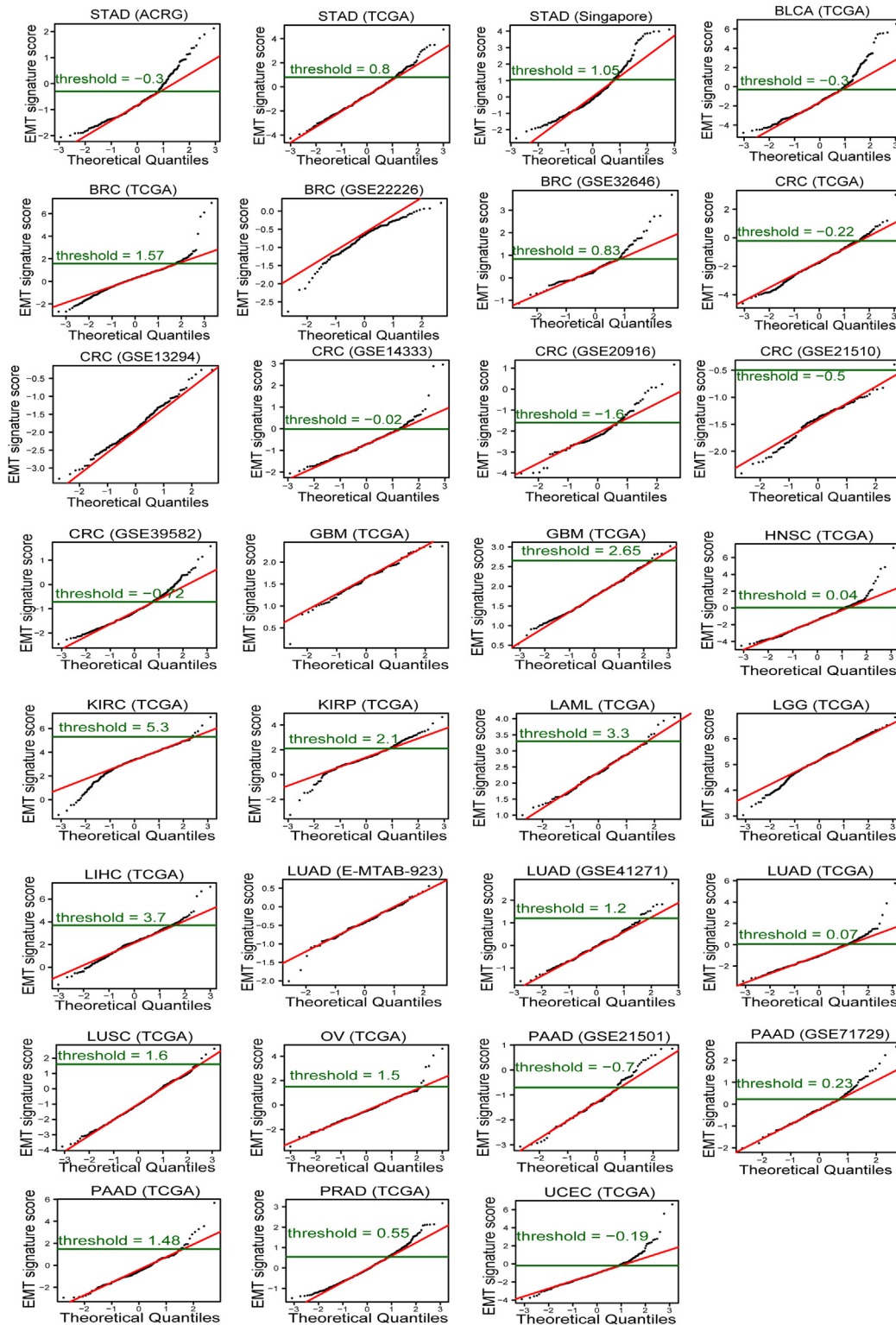
Supplementary Figure 5. Quantile-quantile (q-q) plots for EMT signature scores across 31 tumor-transcriptome datasets. Sample (y-axis) versus theoretical (x-axis) quantiles of the EMT signature scores for the indicated tumor transcriptome datasets. Red lines pass through the first and third theoretical quartiles in each plot. The EMT signature score thresholds where the theoretical q-q line and the positive tail intersect (dark green lines) were used to classify samples into EMT (above the threshold) and non-EMT (below the threshold) groups. Five graphs do not show a threshold value because a positive tail was not found.

A

B

C

NAPRT IHC intensity	EMT	non-EMT
Neg(0)	27	33
Pos(1,2,3)	20	98

Fisher's exact test $p = 0.000122$

D

E

F

Supplementary Figure 6. EMT-associated down-regulation of NAPRT is observed in primary and metastatic gastric tumors. (*A*) Classification of the 178 TMA tumor samples according to their EMT gene expression signatures. Rows represent genes belonging to the EMT signature (149 upregulated genes on the top, 161 downregulated genes on the bottom). EMT-subtype tumors were detected using unsupervised hierarchical clustering with average linkage based on the Euclidean distance of the gene expression values. (*B*) Comparison of *NAPRT* expression levels in EMT and non-EMT tumor samples in *A*. The *p*-value from Wilcoxon rank sum test is displayed for the comparison. Box-and-whisker plots represent the median (middle line), the first quartile (lower bound line), the third quartile (upper bound line), and the ± 1.5 interquartile range (whisker lines), with raw data overlaid. (*C*) Contingency table displaying distribution of samples in *A* according to their EMT status and NAPRT expression levels measured by IHC. (*D*) A scatter plot of gene expression correlations for tumor samples in *A*. A red dashed line represents a regression line. The Pearson correlation coefficients (r) and test *p* values are shown in the plot. (*E*) Immuno-histochemistry staining of NAPRT and E-cadherin in matched primary and liver metastatic gastric tumors. Representative images are shown for three matched samples showing co-depletion of the two indicated proteins in metastatic tumors. Scale bar, 20 mm. (*F*) Representative images are shown for liver (left) and ovarian (right) metastatic tumors that exhibited NAPRT negativity. Scale bar, 20 mm.
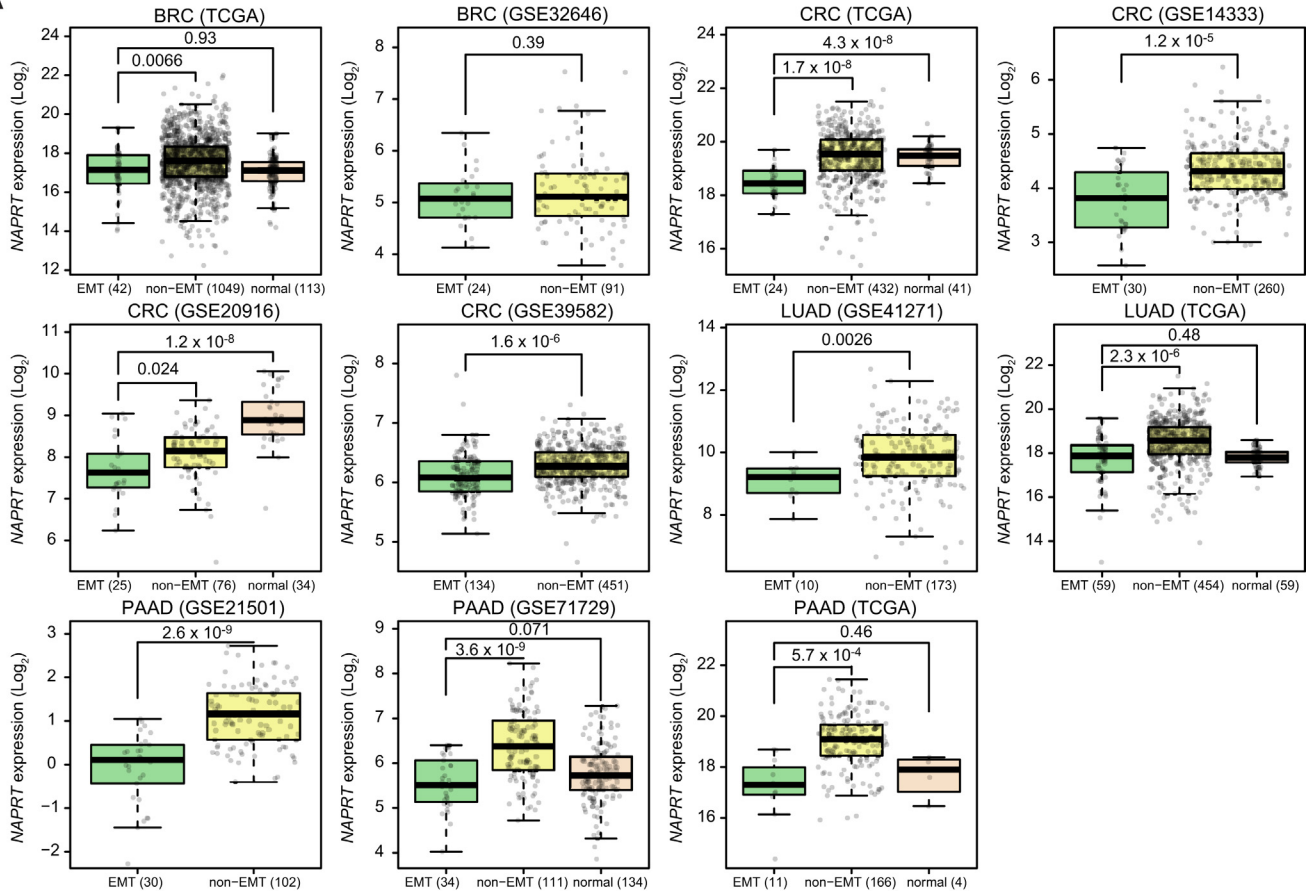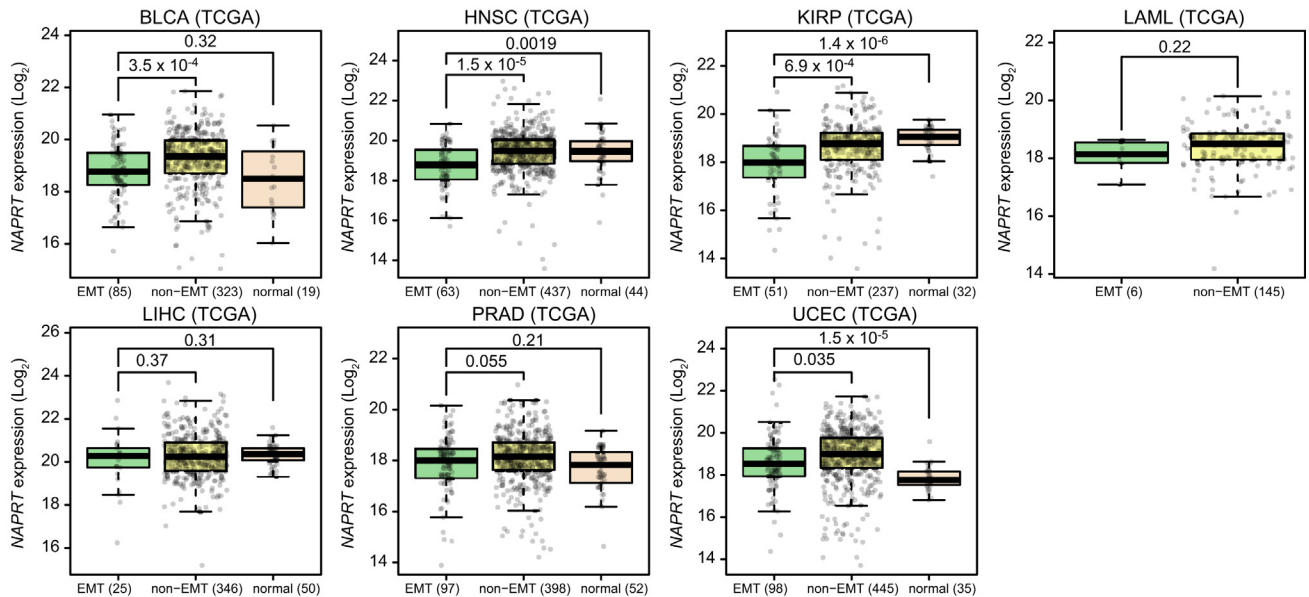
Supplementary Figure 7. Nicotinic acid phosphoribosyltransferase (*NAPRT*) expression levels in tumor samples. (*A-B*) The indicated transcriptome datasets (size > 100, EMT > 3%) were used to compare *NAPRT* expression levels between samples classified as EMT or non-EMT on the basis of their EMT signature scores. Fourteen of the 21 datasets were eligible for meta-analysis (*A*), and each of the seven other datasets solely represents a tumor type (*B*). See also Figure 4*C* for three datasets of stomach adenocarcinoma. Group sizes for each cohort are presented in parentheses. Student's t-test *p*-values that reflect comparisons between EMT and non-EMT tumor samples and between EMT tumor and normal samples, respectively, are shown above the plots. Box-and-whisker plots show the median (middle bound line), the first quartile (lower bound line), the third quartile (upper bound line), and the ±1.5 interquartile range (whisker lines), with raw data overlaid. BLCA, bladder urothelial carcinoma; BRC, breast cancer; CRC, colorectal cancer; HNSC, head and neck squamous cell carcinoma; KIRP, kidney renal papillary cell carcinoma; LAML, acute myeloid leukemia; LIHC, liver hepatocellular carcinoma; LUAD, lung adenocarcinoma; PAAD, pancreatic ductal adenocarcinoma; PRAD, prostate adenocarcinoma; UCEC, uterine corpus endometrial carcinoma.
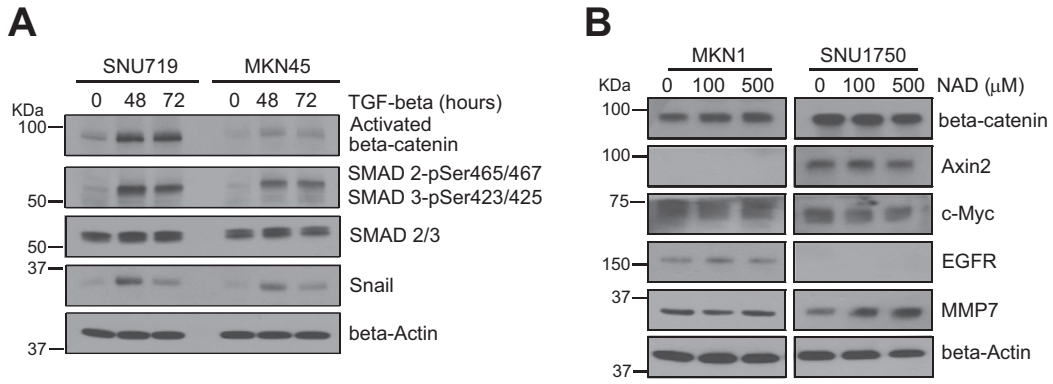
Supplementary Figure 8. TGF-β activates β-catenin signaling, and NAPRT-dependent suppression of β-catenin expression is independent of nicotinamide adenine dinucleotide (NAD) biosynthesis. (*A*) The accumulation of the indicated proteins was determined by western blot analysis following the exposure of non-EMT gastric cancer cell lines to tumor growth factor (TGF)-β (20 ng/mL) for the indicated time. beta-actin was utilized as a loading control. (*B*) Western blot analysis of β-catenin target expression in EMT gastric cancer cell lines MKN1 and SNU1750 after treatment with NAD at the indicated concentrations. EGFR, epidermal growth factor receptor; MMP7, matrix metallopeptidase 7.